Silencing of genes by promoter hypermethylation shapes tumor microenvironment and resistance to immunotherapy in clear-cell renal cell carcinomas

Xiaofan Lu, Yann-alexandre Vano, Xiaoping Su, Alexandra Helleux, Véronique Lindner, Roger Mouawad, Jean-Philippe Spano, Morgan Roupret, Eva Comperat, Virginie Verkarre, et al.

Cell Reports
Medicine

Article

Silencing of genes by promoter hypermethylation shapes tumor microenvironment and resistance to immunotherapy in clear-cell renal cell carcinomas

Graphical abstract

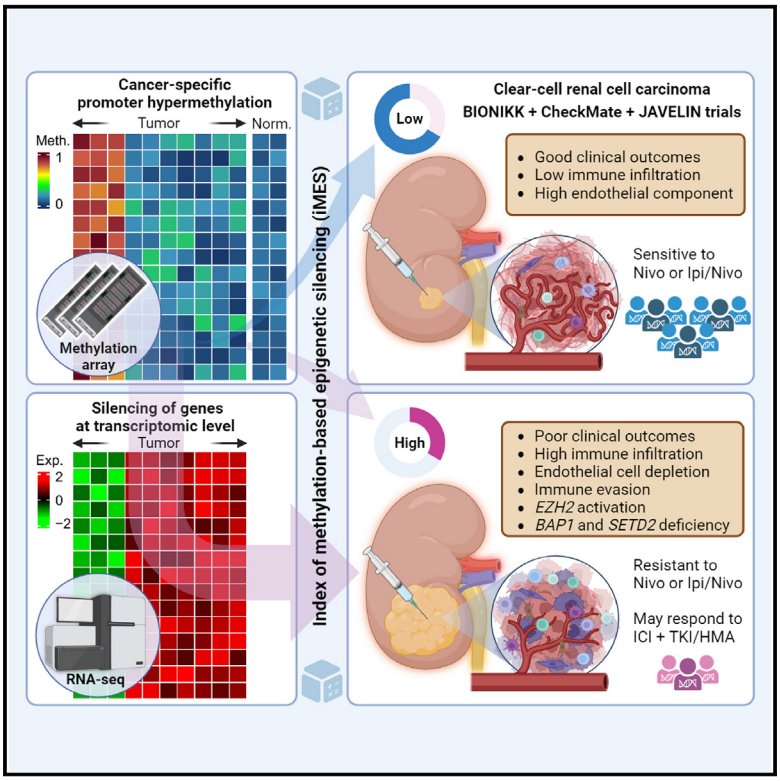

Highlights

- Gene silencing influences both ccRCC aggressiveness and microenvironment
- A methylation index (iMES) reliably predicts ICI treatment outcomes in ccRCC
- Elevated iMES correlates with *EZH2* activation and *BAP1*/*SETD2* deficiency
- iMES and angiogenesis jointly impact response to immunotherapy in ccRCC

Authors

Xiaofan Lu, Yann-Alexandre Vano, Xiaoping Su, ..., Catherine Sautes-Fridman, Stéphane Oudard, Gabriel G. Malouf

Correspondence

maloufg@igbmc.fr

In brief

Lu et al. develop an index of methylation-based epigenetic silencing (iMES) signature and unveils its potential to predict immunotherapy outcomes in clear-cell renal cell carcinoma (ccRCC), unlocking the intricate relationship between the tumor microenvironment and promoter methylation. Intriguingly, endothelial cell depletion corresponds to *VEGF* pathway methylation, proposing a link between iMES, angiogenesis, and immunotherapy response in ccRCC patients.

Lu et al., 2023, Cell Reports Medicine *4*, 101287
November 21, 2023
https://doi.org/10.1016/j.xcrm.2023.101287

CellPress

Cell Reports Medicine

CellPress
OPEN ACCESS

Article

Silencing of genes by promoter hypermethylation shapes tumor microenvironment and resistance to immunotherapy in clear-cell renal cell carcinomas

Xiaofan Lu,[1,16] Yann-Alexandre Vano,[2,3,16] Xiaoping Su,[4,16] Alexandra Helleux,[1] Véronique Lindner,[5] Roger Mouawad,[6] Jean-Philippe Spano,[6] Morgan Rouprêt,[7] Eva Compérat,[8] Virginie Verkarre,[9] Cheng-Ming Sun,[3] Mostefa Bennamoun,[10] Hervé Lang,[11] Philippe Barthelemy,[12] Wenxuan Cheng,[13] Li Xu,[13] Irwin Davidson,[1] Fangrong Yan,[13] Wolf Hervé Fridman,[3] Catherine Sautes-Fridman,[3] Stéphane Oudard,[3,15,17] and Gabriel G. Malouf[1,14,15,17,18,*]

[1]Department of Cancer and Functional Genomics, Institute of Genetics and Molecular and Cellular Biology, CNRS/INSERM/UNISTRA, 67400 Illkirch, France
[2]Department of Medical Oncology, Hôpital Européen Georges Pompidou, Institut du Cancer Paris CARPEM, AP-HP, Université Paris Cité, Paris, France
[3]Centre de Recherche Cordeliers, INSERM 1138, Université de Paris Cité, Sorbonne Université, Equipe labellisée Ligue contre le Cancer, 75006 Paris, France
[4]Department of Bioinformatics and Computational Biology, The University of Texas MD Anderson Cancer Center, Houston, TX, USA
[5]Department of Pathology, Strasbourg University Hospital, Strasbourg, France
[6]Department of Medical Oncology, Sorbonne University, AP-HP, Hôpital Pitié-Salpêtrière, Paris, France
[7]Sorbonne University, GRC 5 P, UKredictive Onco-Uro, AP-HP, Urology, Pitié-Salpêtrière Hospital, 75013 Paris, France
[8]Department of Pathology, Sorbonne University, AP-HP, Hôpital Tenon, Paris, France
[9]Department of Pathology, Hôpital Européen Georges Pompidou, Institut du Cancer Paris CARPEM, AP-HP, Université Paris Cité, Paris, France
[10]Department of Medical Oncology, Institut Mutualiste Montsouris, Paris, France
[11]Department of Urology, Strasbourg University Hospital, Strasbourg, France
[12]Department of Medical Oncology, Strasbourg University, Institut de Cancérologie de Strasbourg, Strasbourg, France
[13]Research Center of Biostatistics and Computational Pharmacy, China Pharmaceutical University, Nanjing, P.R. China
[14]Department of Medical Oncology, Strasbourg University, Institut de Cancérologie de Strasbourg, Strasbourg, France
[15]Senior author
[16]These authors contributed equally
[17]These authors contributed equally
[18]Lead contact
*Correspondence: maloufg@igbmc.fr
https://doi.org/10.1016/j.xcrm.2023.101287

SUMMARY

The efficacy of immune checkpoint inhibitors varies in clear-cell renal cell carcinoma (ccRCC), with notable primary resistance among patients. Here, we integrate epigenetic (DNA methylation) and transcriptome data to identify a ccRCC subtype characterized by cancer-specific promoter hypermethylation and epigenetic silencing of Polycomb targets. We develop and validate an index of methylation-based epigenetic silencing (iMES) that predicts primary resistance to immune checkpoint inhibition (ICI) in the BIONIKK trial. High iMES is associated with *VEGF* pathway silencing, endothelial cell depletion, immune activation/suppression, *EZH2* activation, *BAP1/SETD2* deficiency, and resistance to ICI. Combination therapy with hypomethylating agents or tyrosine kinase inhibitors may benefit patients with high iMES. Intriguingly, tumors with low iMES exhibit increased endothelial cells and improved ICI response, suggesting the importance of angiogenesis in ICI treatment. We also develop a transcriptome-based analogous system for extended applicability of iMES. Our study underscores the interplay between epigenetic alterations and tumor microenvironment in determining immunotherapy response.

INTRODUCTION

Clear-cell renal cell carcinoma (ccRCC) is the predominant kidney cancer, responsible for numerous cancer-related deaths.[1] Somatic *VHL* mutations are well known, but recent studies have identified new mutations related to chromatin modification and intratumor diversity, spurring the development of various Food and Drug Administration-approved therapies for metastatic RCC.[2] Based on recent randomized phase III trials, current guidelines recommend first-line treatment with dual immune checkpoint inhibition (ICI) or a combination of vascular endothelial growth factor (VEGF) receptor tyrosine kinase inhibitor (TKI) and anti-PD-1 ICI.[3]

The CheckMate-214 trial showed a 42% response rate with ipilimumab plus nivolumab (Ipi/Nivo), but nearly 20% of patients showed disease progression early on.[4] While various methods, including single-cell RNA sequencing (RNA-seq), have sought potential biomarkers, bulk RNA profiling has identified distinct RCC molecular subtypes, which were evaluated in several clinical trials.[4–8] However, transcriptomic signatures from trials such as IMmotion150 and JAVELIN Renal 101 have shown limited predictive value for Ipi/Nivo and nivolumab monotherapies, making biomarker identification for ccRCC immunotherapy challenging.[5,9–11]

We recently defined a ccRCC subgroup with an enhancer demethylator phenotype (*TED*$^+$), linked to a distinct transcriptome program, poor prognosis, and ICI resistance.[12] This work has highlighted the critical role of epigenetic alterations—specifically, alterations in DNA methylation—and their interplay with the transcriptome landscape in future biomarker studies for ccRCC.[13] DNA methylation in promoter CpG islands (CGIs) serves as an epigenetic regulator of gene expression. The technology is advanced enough to diagnose cancer from blood samples and produce trait-associated methylation profile scores (MPSs).[14] Importantly, MPSs are evolving to stratify disease risks, including cancer, and are robust across different ancestries.[15–17]

Given RNA-based biomarkers' limited success and DNA methylation's potential, we explored integrating epigenetic (i.e., promoter methylation) and transcriptomic data to identify reliable ICI response predictors in ccRCC, using the BIONIKK clinical trial as our basis. The BIONIKK trial, guided by the Descartes classifications, is the first to validate biomarker-driven patient selection in ccRCC.[18,19] In several ccRCC cohorts we investigated epigenetic silencing through cancer-specific promoter hypermethylation, which we found to be associated with tumor microenvironment (TME) composition, and we further developed and validated an index of methylation-based epigenetic silencing (iMES), an MPS that could help predict Ipi/Nivo treatment outcomes in ccRCC. Intriguingly, we discovered an inverse correlation between iMES and endothelial cell signatures, suggesting that response to ICI in ccRCC might necessitate functional vasculatures and that this might be dampened by hypoxia.

RESULTS

Epigenetic silencing is associated with *SETD2* mutations, 9p loss, and tumor aggressiveness

Using the Illumina 450K array, we studied 301 ccRCC tumors and 160 normal kidney samples from The Cancer Genome Atlas (TCGA) (Figure 1). We filtered out probes with a median β value above 0.2 in normal samples, leaving 76,239 probes mapping to 12,343 genes. Integrative analysis identified 493 genes epigenetically silenced through cancer-specific DNA hypermethylation at promoter CGIs (Table S1).

Through unsupervised clustering on 101 frequently methylated genes (>20%), we identified two ccRCC subtypes: EPI-C1 (n = 78) and EPI-C2 (n = 223) (Figure 2A). Interestingly, EPI-C1 had a significantly higher proportion of our previously identified *TED*$^+$ phenotype compared to EPI-C2 (38.5% vs. 16.6%, $p < 0.001$). These two subtypes were tightly associated with patients' clinical outcomes ($p < 0.001$; Figure 2B). Of note, 75 out of the 101 silenced genes (74.3%) were found to be prognostic using univariate analysis, and all were associated with an increased risk of death (hazard ratio [HR] > 1, false discovery rate [FDR] < 0.05; Figure S1), suggesting that epigenetic silencing had broad prognostic relevance in ccRCC.

EPI-C1 was strongly associated with advanced tumor grades (G1 + G2: 23.4% vs. 52.5%; G3 + G4: 76.7% vs. 47.5%; $p < 0.001$) and stage (I + II: 26% vs. 69.4%; III + IV: 74.1% vs. 30.6%; $p < 0.001$) compared to EPI-C2 (Figures 2C and 2D; Table S2). Since ccRCC with sarcomatoid and rhabdoid differentiation (sccRCC/rccRCC) forms the most aggressive clinicopathologic phenotypes, we evaluated those cases with reviewed pathology reports.[20,21] We found that among 29 sccRCCs, 13 cases belonged to EPI-C1, indicating that EPI-C1 was significantly enriched in sccRCC compared to EPI-C2 (16.7% vs. 7.2%, $p = 0.026$). No enrichment was observed regarding rccRCCs (Table S2).

Given the reported correlation between 9p deletion and the aggressiveness of RCC,[22] we investigated the TCGA-KIRC cohort and revealed more frequent 9p loss in the EPI-C1 compared to EPI-C2 (39 [50.6%] vs. 31 [14.1%], $p < 0.0001$; Figure 2A). In addition, SET Domain Containing 2 (*SETD2*) was identified as the only gene whose mutations was frequently enriched in EPI-C1 compared to EPI-C2 (22 [37.3%] vs. 16 [8.7%], $p < 0.001$, FDR <0.001; Table S3).

To explore the role of cancer-specific hypermethylation in distinguishing the malignancy of tumors, we collected an independent cohort of ccRCC (PSL cohort, n = 46) that was enriched for high-grade tumors (G4: n = 27, 58.7%) and tumors with metastatic presentation at baseline (M1: n = 9, 19.6%). Owing to the lack of adjacent normal controls, we used a second dataset (GSE61441) to establish a consensus of cancer-specific promoter hypermethylated probes.[23] We identified 75,721 probes (Figure S2A), with 72,110 probes overlapping between TCGA-KIRC (94.6%) and GSE61441 (95.2%) cohorts (Figure S2B), indicating stable cancer-specific hypermethylation among ccRCC tumors (representation factor 5.7, $p < 0.001$).

Gene-level analysis with 72,110 probes confirmed two subtypes in the PSL cohort (Figure S2C). EPI-C1 showed worse clinical outcomes ($p = 0.0001$; Figure S2D) and was linked to advanced stages and grades (Figures S2E and S2F; Table S4). Consistently, aggressive EPI-C1 harbored all detected 9p loss as compared to EPI-C2 (7 [28%] vs. 0, $p = 0.011$; Figure S2C). Furthermore, higher proportions of sccRCCs (52% vs. 33.3%), rccRCCs (20% vs. 4.8%), and necrosis (36% vs. 19%) were observed in EPI-C1 compared to EPI-C2, without statistical significance (all $p > 0.1$).

Epigenetic silencing converged to *EZH2* overexpression, *PRC2* hypermethylation, and *BAP1* loss

We then examined the DNA methylation differences between two epigenetic subtypes. In the TCGA-KIRC cohort, we revealed 2,363 hypermethylated probes in EPI-C1 and only 14 in EPI-C2 (Table S5). These were primarily located in promoter CGIs (fold change 1.92, $p < 0.001$; Figure S3A) and enriched in Polycomb repressive complex 2 (*PRC2*) targets (FDR < 0.001; Figure S3B).

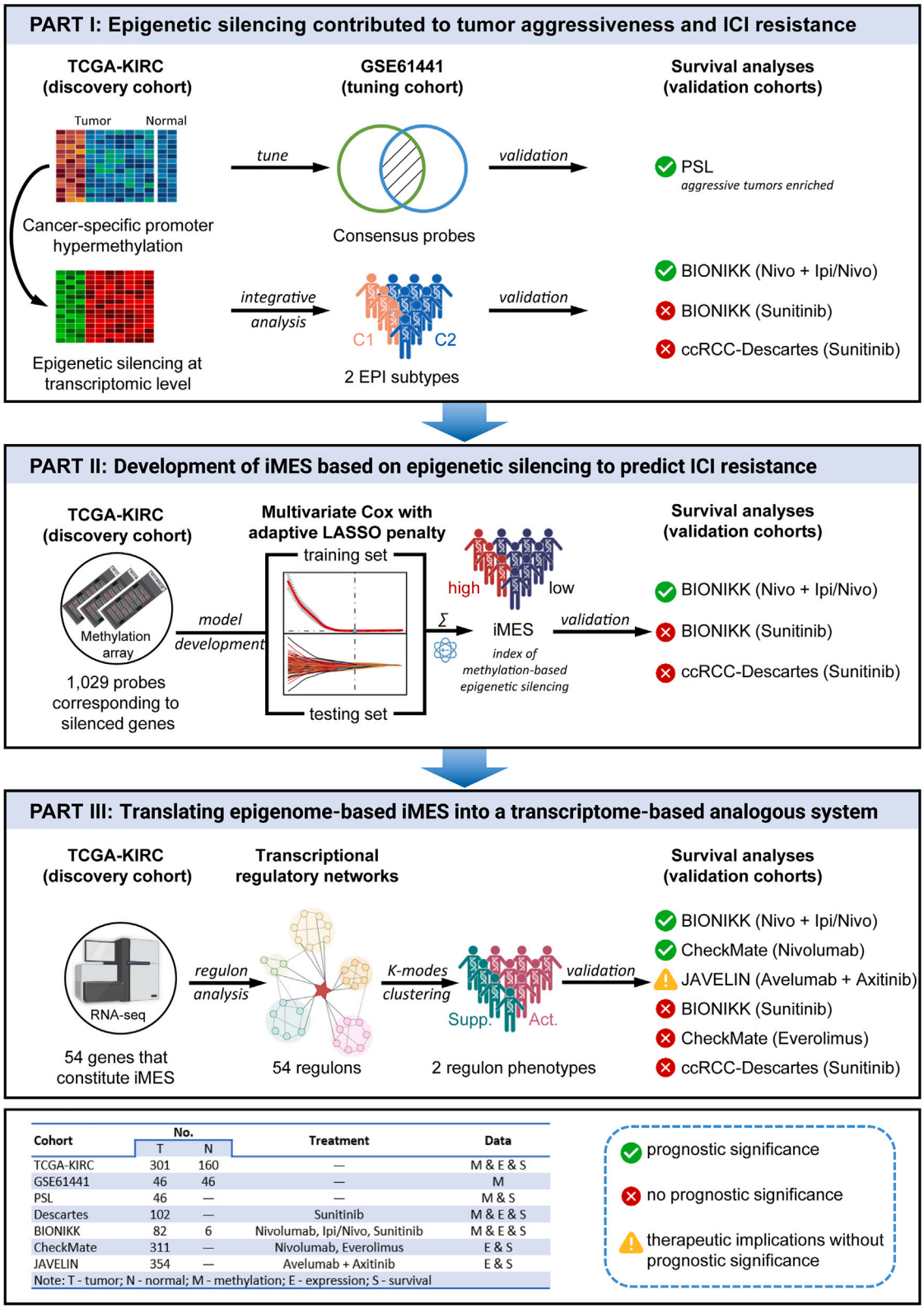

Cohort	No.		Treatment	Data
	T	N		
TCGA-KIRC	301	160	—	M & E & S
GSE61441	46	46	—	M
PSL	46	—	—	M & S
Descartes	102	—	Sunitinib	M & E & S
BIONIKK	82	6	Nivolumab, Ipi/Nivo, Sunitinib	M & E & S
CheckMate	311	—	Nivolumab, Everolimus	E & S
JAVELIN	354	—	Avelumab + Axitinib	E & S

Note: T - tumor; N - normal; M - methylation; E - expression; S - survival

Figure 1. Flow diagram of the study

Flow diagram illustrating the study's logical progression from initial epigenetic silencing to the development of the epigenome-based iMES and transcriptome-based systems.

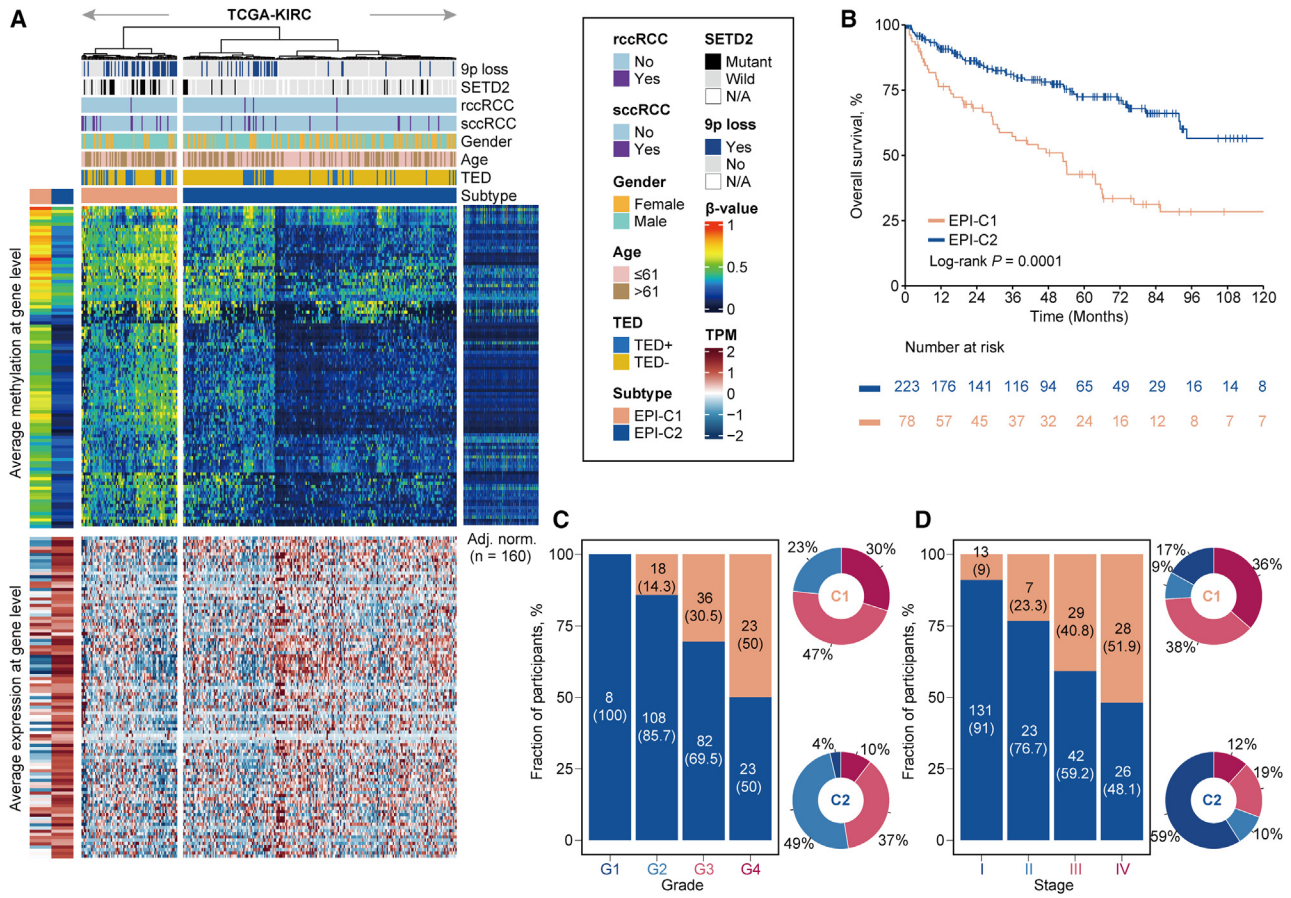

Figure 2. Association between epigenetic silencing by DNA methylation and tumor aggressiveness of ccRCC

(A) Heatmap of methylation and gene expression profiles in TCGA cohort, including annotations for adjacent normal tissues and clinical features.

(B) Kaplan-Meier curves depicting OS rates of epigenetic subtypes.

(C) Bar plots (actual sample size shown within parentheses below the percentage) and pie charts showing the association between two epigenetic subtypes and tumor grade.

(D) Same as (C) but for tumor stage.

We identified 1,143 regions that were hypermethylated in EPI-C1, with only eight in EPI-C2 (Table S6), and these regions were also enriched in *PRC2* targets (FDR < 0.001; Figure S3C). Notably, hypermethylation of Polycomb targets was reconciled with overexpression of enhancer of zeste 2 Polycomb repressive complex 2 subunit (*EZH2*) in EPI-C1 compared to EPI-C2 (fold change 1.25, p < 0.001, FDR < 0.001; Figure 3A). *EZH2* is a key component of *PRC2* and its overexpression can lead to increased activity of *PRC2*, resulting in hypermethylation of target genes, including *PRC2* itself.

Intriguingly, overexpression of *EZH2* has been linked to *BAP1* loss.[24] Although BAP1 mutations were not strongly linked to the epigenetic subtypes, its role in chromatin accessibility has been underscored in a recent study.[25] To explore this, we identified regions with reduced chromatin accessibility in *BAP1*-mutant tumors and developed a *BAP1*-loss-driven chromatin repression signature (*BAP1*-LCR). This signature was inversely correlated with *EZH2* expression (r = −0.24, p < 0.0001) and diminished in EPI-C1 (p < 0.001; Figure 3B), suggesting that *BAP1* loss, potentially encompassing more than mere mutation, may contribute to the epigenetic silencing observed in ccRCC.

Epigenetic silencing contributed to potential ICI resistance

Our gene set enrichment analysis (GSEA) showed that the EPI-C1 in the TCGA-KIRC cohort was associated with increased inflammatory response, epithelial-mesenchymal transition (EMT), and the IL-6/JAK/STAT3 Hallmark pathways (all, normalized enrichment score [NES] > 1.5, FDR < 0.05; Figure 3C). The enrichment of sarcomatoid in EPI-C1 was consistent with the role of EMT in sarcomatoid and rhabdoid changes. Activation of the IL-6/JAK/STAT3 pathway suggests a higher likelihood of immune evasion in EPI-C1,[26] backed by higher Tumor Immune Dysfunction and Exclusion (TIDE) scores (p = 0.028; Figure 3D) and more predicted non-responders (p = 0.022; Figure 3E).[27] Previous studies have reviewed the association between alterations in *PRC2* function, including overexpression of *EZH2*, hypermethylation of *PRC2*, and exhausted T cells that cause ICI

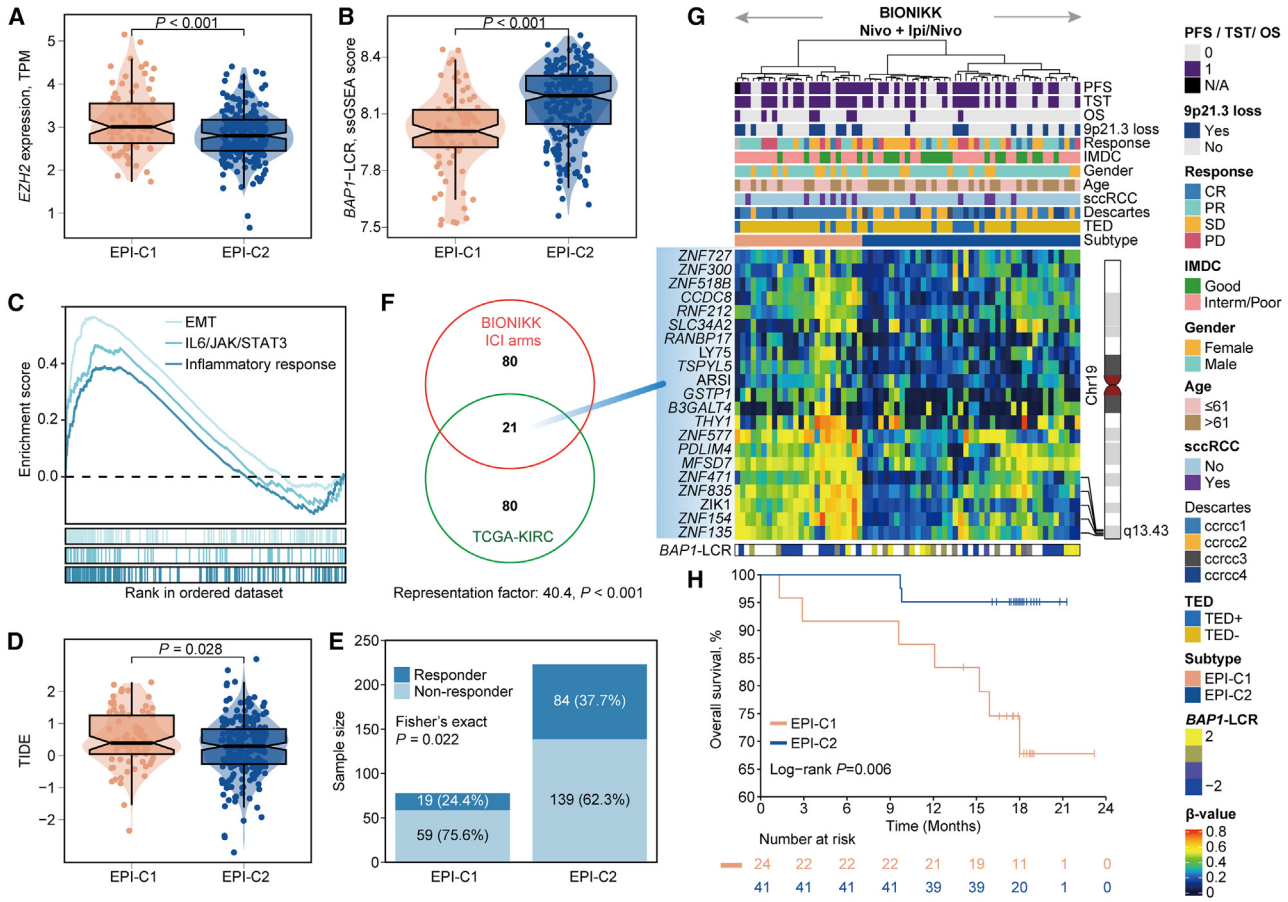

Figure 3. Epigenetic silencing by DNA methylation and its role in primary resistance to ICI treatment of ccRCC

(A) Violin plot of EZH2 expression between epigenetic subtypes of TCGA cohort.
(B) Violin plot of *BAP1*-LCR levels between epigenetic subtypes of TCGA cohort.
(C) GSEA of activated pathways in EPI-C1 of TCGA cohort.
(D) Violin plot of TIDE scores between epigenetic subtypes of TCGA cohort.
(E) Stacked bar plot of TIDE-predicted ICI responder fractions in two epigenetic subtypes of TCGA cohort.
(F) Venn diagram of the intersection of epigenetically silenced genes between TCGA-KIRC and BIONIKK's ICI arms.
(G) DNA methylation landscape of epigenetically silenced genes in two epigenetic subtypes in BIONIKK's ICI arms.
(H) Kaplan-Meier curves depicting OS rates of epigenetic subtypes in BIONIKK's ICI arms.

resistance.[28] Based on these findings, we proposed that epigenetic silencing may contribute to ICI resistance in ccRCC.

Using BIONIKK trial data,[19] we conducted Illumina EPIC profiling for 65 samples from patients who received treatment with either nivolumab (arm A: n = 19) or a combination of Ipi/Nivo (arm B: n = 46), as well as 17 samples from patients treated with sunitinib (arm C). We also profiled methylomes of six adjacent normal kidneys to assess cancer-specific hypermethylation. Additionally, we performed RNA-seq on 95 samples with good RNA quality, including 28 from the nivolumab arm, 48 from the Ipi/Nivo arm, and 19 from the sunitinib arm. Among these samples, 48 samples had both DNA methylation and expression data, including 12 from the nivolumab arm, 27 from the Ipi/Nivo arm, and 9 from the sunitinib arm.

Our integrative analysis identified 341 silenced genes, with 101 frequently methylated (Table S7). Among these genes, 21 (20.8%) overlapped with those identified in the TCGA-KIRC cohort (representation factor 40.4, $p < 0.001$; Figure 3F). Notably, we observed a significant enrichment of the cytogenetic region 19q13.43 for these genes (FDR < 0.0001), which includes zinc-finger proteins such as *ZNF135*, *ZNF154*, *ZNF471*, *ZNF835*, and *ZIK1*. Through supervised clustering, we identified two epigenetic subtypes (EPI-C1, n = 24; EPI-C2, n = 41) among patients receiving ICI treatment (Figure 3G). Patients with EPI-C1 were associated with significantly poorer overall survival (OS) ($p = 0.006$; Figure 3H). The median survival for progression-free survival (PFS) (13.1 vs. 7.3 months) and time to second treatment (TST) (20.8 vs. 10.9 months) was nearly double in EPI-C2 compared to EPI-C1, although no statistical significance was reached (both $p > 0.1$; not shown). Of note, EPI-C1 (16, 69.6%; one had no record for PFS) showed a slightly higher proportion of ICI non-responders compared to EPI-C2 (19, 46.3%) (progressive disease, stable disease, or partial response with PFS time of less than 12 months; $p = 0.062$). No statistical association

was observed between epigenetic subtypes and other clinical features (all $p > 0.1$; Table S8) but marginally associated with Descartes classifications ($p = 0.076$). Interestingly, EPI-C2 was highly enriched for the pro-angiogenic ccrcc2 group (14 [34.1%] vs. 3 [12.5%], $p = 0.079$). We also observed a marginal enrichment of 9p loss, specifically at the focal-level region of 9p21.3, in the EPI-C1 subgroup compared to EPI-C2 (11 [45.8%] vs. 9 [22%], $p = 0.055$; Figure 3G).

In the BIONIKK cohort, we discovered 320 hypermethylated probes and 662 regions for EPI-C1, but none for EPI-C2 (Tables S9 and S10). These were enriched in promoter CGIs (fold change 3.93, $p < 0.001$; Figure S4A) and *PRC2* targets (FDR < 0.001; Figures S4B and S4C), similar to findings in the TCGA-KIRC cohort. Consistently, we found an inverse correlation between the *BAP1*-LCR signature and *EZH2* expression ($r = -0.29$, $p = 0.071$) as well as lower signature score in EPI-C1 compared to EPI-C2 ($p = 0.003$; Figure 3G). Supervised clustering identified two epigenetic subtypes in patients who received TKI treatment (Figure S5A); however, no prognostic relevance was observed (all $p > 0.6$; Figure S5B). Despite the small sample size of the BIONIKK TKI arm, we investigated a larger cohort, the ccRCC-Descartes cohort, which included 102 patients with metastatic ccRCC who were treated with the first-line TKI sunitinib.[18] Likewise, statistical significance was not reached for survival analyses in the two epigenetic subtypes ($p > 0.05$; Figures S6A and S6B). These results suggested that epigenetic silencing may play a role in shaping aggressiveness and resistance to ICI in ccRCC.

Development and validation of an iMES that was relevant to ICI resistance

To identify potential prognostic factors and predict the outcomes of patients receiving ICI treatment, we analyzed promoter CGI probes corresponding to genes that were silenced in the TCGA-KIRC cohort. Probes that had a constant methylation status were filtered out and those methylated in at least 5% of the samples were kept, resulting in a total of 1,029 probes. To prevent overfitting, the TCGA discovery cohort was split into a training set ($n = 240$) with 80% of the samples and an internal testing set ($n = 61$) with 20% of the remaining samples. Using a multivariate Cox regression model with the adaptive least absolute shrinkage and selection operator (adaLASSO) penalty, we determined the optimal λ value when the partial likelihood deviance reached the minimum value based on 10-fold cross-validation (Figure 4A). Fifty-eight probes with non-zero adaLASSO coefficients were selected and used to develop a methylation-based epigenetic silencing index, referred to as iMES (Figure 4B and S7). We calculated an iMES for each sample via a linear combination of these probes, weighted by their coefficients (Table S11).

The patients were divided into iMES-high and iMES-low groups based on the upper tertile of the iMES in the training set of the TCGA-KIRC cohort. In this set, a higher iMES was significantly associated with worse OS (HR = 3.86, 95% confidence interval [CI] 3.06–4.87, $p < 0.001$; log rank $p < 0.001$; Figure S8A). The iMES was then evaluated on the internal testing set, which comprised unseen data that came from the same distribution as the training set. In this set, higher iMES was also significantly associated with worse OS (HR = 2.79, 95% CI 1.97–3.95, $p < 0.001$; log rank $p < 0.001$; Figure S8B), indicating less likelihood of overfitting and a good ability to generalize to new situations. We then applied iMES to the entire TCGA-KIRC cohort, whereby it showed a significant association with OS (HR = 3.51, 95% CI 2.91–4.24, $p < 0.001$; log rank $p < 0.001$; Figure 4C). The time-dependent receiver-operating characteristic (ROC) analysis indicated that iMES had a good discriminative ability, with time-dependent area under the curve (AUC) values of 0.86 at 1 year, 0.86 at 3 years, 0.87 at 5 years, and 0.91 at 10 years (Figure 4D).

To assess the potential of iMES as a prognostic indicator for patients receiving ICI treatment, iMES was calculated for each sample in the BIONIKK cohort. We found that a higher iMES was strongly associated with an increased risk of poor PFS (HR = 1.45, 95% CI 1.07–1.97, $p = 0.018$), TST (HR = 1.56, 95% CI 1.12–2.17, $p = 0.008$), and OS (HR = 2.35, 95% CI 1.18–4.66, $p = 0.015$) for patients in the nivolumab and Ipi/Nivo arms. Furthermore, iMES was able to stratify patients into iMES-high ($n = 22$) and iMES-low ($n = 43$) groups with significantly different prognoses for PFS ($p = 0.001$; Figure 4E), TST ($p < 0.001$; Figure 4F), and OS ($p = 0.019$; Figure 4G). The iMES-high group significantly enriched in ICI non-responders (18, 85.7%) compared to the iMES-low group (17, 39.5%) ($p < 0.001$). Consistently, non-responders had significantly higher iMES compared to responders ($p = 0.007$). Time-dependent ROC analysis revealed that iMES had good discriminative ability for both short-term and long-term OS prediction (average AUC: 0.91), but its performance in predicting TST was limited to the short term (average AUC: 0.83 within 3 months) (Figure 4H). While the overall effectiveness of the treatment may be difficult to evaluate due to low AUC for long-term TST prediction (average AUC: 0.68), iMES may be useful to identify patients at high risk for experiencing TST early, which could be valuable in making treatment decisions to consider alternative treatment options or closer monitoring.

No statistical association was observed between iMES and patient outcomes in both the BIONIKK and ccRCC-Descartes TKI cohorts (all $p > 0.05$; Figures S9A and S9B), suggesting that iMES may be most useful in predicting resistance to ICI in ccRCC patients treated in first line.

iMES was an independent prognostic factor

We then investigated whether iMES could serve as an independent prognostic factor in localized and metastatic ccRCCs (Figure 4I). We found that iMES remained a significant independent prognostic factor after adjusting for other major clinical prognostic features in the TCGA-KIRC cohort ($p < 0.001$). In the PSL cohort, iMES was not significant ($p = 0.561$), possibly due to the limited sample size. Despite this, the data reinforced the evidence that iMES was closely associated with aggressive tumor features. Additionally, iMES remained an independent prognostic factor in the ICI arms of the BIONIKK cohort ($p < 0.05$ for all events of interest). These findings suggest a potential for iMES to augment the International Metastatic RCC Database Consortium risk score in prognostication, particularly for patients receiving immunotherapy. However, this preliminary observation requires further validation in larger cohorts.

CellPress
OPEN ACCESS

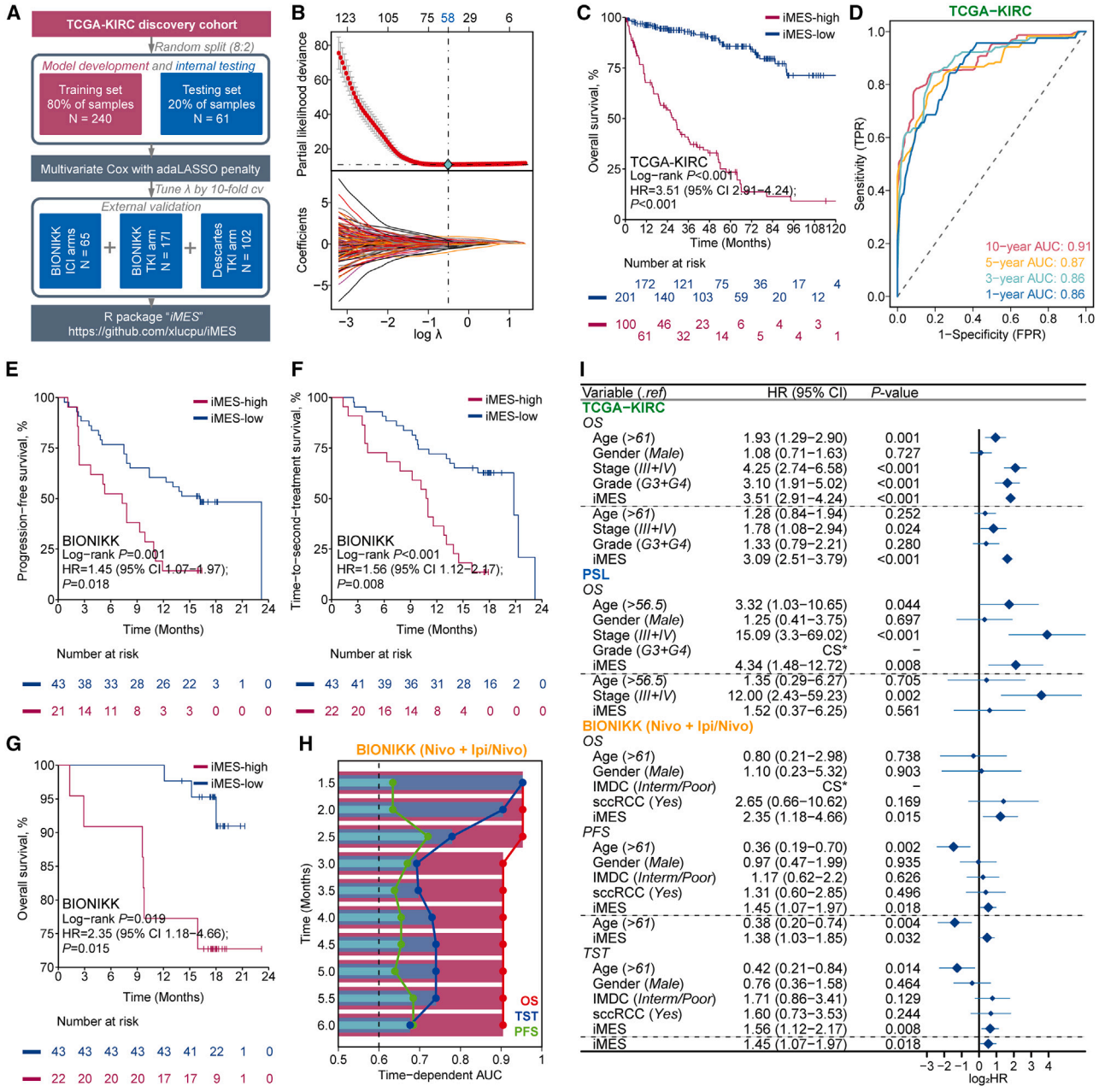

Figure 4. Development and validation of an iMES

(A) Flow chart.

(B) Selection of λ in the adaLASSO model. The partial likelihood deviance was plotted vs. log(λ) (top panel), and a coefficient parole plot was produced against the log(λ) sequence (bottom panel).

(C) Kaplan-Meier survival curve depicting OS rates of two iMES groups in TCGA cohort.

(D) Time-dependent ROC curves of iMES in TCGA cohort. TPR, true positive rate; FPR, false positive rate.

(E) Kaplan-Meier curves of PFS for patients stratified by iMES in BIONIKK's ICI arms.

(F) Same as (E) but for TST.

(G) Same as (E) but for OS.

(H) Time-dependent ROC curves of iMES within 6 months after treatment in BIONIKK's ICI arms.

(I) Forest plot displaying hazard ratios in univariate (above the dashed line) and multivariate (below the dashed line) analyses. CS, complete separation—outcome variable completely separates a predictor variable with inaccurate estimation.

iMES was associated with high immune infiltration and epithelial depletion

To decipher iMES's biological underpinings, we performed GSEA on samples with high and low iMES in the TCGA-KIRC cohort and BIONIKK's ICI arms. High-iMES samples were significantly enriched in pathways related to inflammatory response, interferon-γ response, EMT, and the IL-6/JAK/STAT3 signaling (NES > 1.5, p < 0.05, FDR <0.05). Similar trends were found in the Cancer Cell Line Encyclopedia (CCLE) dataset (Figure 5A).

Given the activation of the interferon-γ pathway in patients with high iMES, we surveyed the ccRCC samples for the expression of immune checkpoint genes, and we investigated the specific immune cell infiltration status and the functional orientation of TME for both cohorts (Figures 5B and 5C). Elevated iMES correlated with increased expression of immune checkpoint genes, including *PDCD1*, *CTLA4*, and *LAG3*, indicating potential immune exhaustion. Additionally, higher iMES was positively correlated with immune activation, such as T cells and $CD8^+$ T cells, and also with suppressive populations, including regulatory T cells (Tregs), tumor-infiltrating Tregs, cancer-associated extracellular matrix (C-ECM), and Wnt/TGF-β. Of note, iMES was inversely correlated with endothelial cells (Figures 5B and 5C), and iMES was significantly lower in Motzer's angiogenic/stromal and angiogenic subtypes as compared to other subtypes (both p < 0.01; Figures S10A and S10B). Further deconvolution using TR4 (Figure 5D), a signature matrix consisting of epithelial, endothelial, fibroblast, and bulk immune cell populations, revealed a positive correlation between iMES and immune cells (both r > 0.25, p < 0.05), while there was an inverse correlation with epithelial cells in both cohorts (both r < −0.35, p < 0.05). Likewise, patients with high iMES had higher proportions of immune and lower endothelial cells compared to those with low iMES in both cohorts (all p < 0.05; Figure 5D).

Considering the tight association between iMES and the TME landscape, we investigated the potential influence of tumor purity, which often correlated with immune infiltration. Our analyses revealed no statistical association between iMES and tumor purity in either the TCGA-KIRC cohort (r = 0.09, p = 0.13) or ICI arms of the BIONIKK cohort (r = 0.12, p = 0.49). Furthermore, we found no prognostic relevance of tumor purity in relation to clinical outcomes in both cohorts (all p ≥ 0.4). Multivariate analysis adjusting for tumor purity demonstrated the independent prognostic value of iMES in both the TCGA-KIRC cohort (OS: HR = 3.57, 95% CI 2.94–4.33, p < 0.0001) and the ICI arms of the BIONIKK cohort (TST: HR = 1.58, 95% CI 1.14–2.19, p = 0.006; PFS: HR = 1.47, 95% CI 1.08–2.0, p = 0.013; OS: HR = 2.32, 95% CI 1.17–4.59, p = 0.016). This suggests that iMES reflects epigenetic changes directly impacting the TME and immunotherapy response.

Endothelial depletion converged with methylation of the VEGF pathway

The decrease in the endothelial cell signature in ccRCC patients with high iMES highlights the importance of exploring VEGF pathways in angiogenesis and tumor progression. We discovered four VEGF-related genes—*FLT4* (36.9%), *PRKCB* (29.6%), *FLT1* (14.9%), and *KDR* (10.3%)—that were frequently methylated (β value >0.2) and co-occurred in their methylation patterns (all, $\log_2$ odds ratio [$\log_2$OR] > 3, FDR < 0.001; Figure 6A and Table S12). The permutation test demonstrated a positive association between iMES and methylation of these genes (all r > 0.3, p < 0.001; Table S13). Consistent with our previous report,[29] the *FLT4* gene had the highest inverse correlation between DNA methylation and expression (r = −0.4, p < 0.001; Figure 6B and Table S13).

In the BIONIK's ICI arms, the same VEGF genes were frequently co-methylated (all except *KDR-PRKCB*, $\log_2$OR > 1.5, FDR < 0.05; Figure 6A and Table S12), including *FLT4* (32.3%), *PRKCB* (72.3%), *FLT1* (41.5%), and *KDR* (38.5%). Of these, *FLT4* (r = 0.18), *PRKCB* (r = 0.17), and *KDR* (r = 0.24) were positively associated with iMES (all p < 0.1; Table S13). We also noted inverse correlations between DNA methylation and expression for *FLT4* and *PRKCB* (Figure 6B and Table S13).

iMES was associated with alterations of chromatin remodeling

Expanding on our previous findings on chromatin alteration in ccRCC, we conducted a thorough regulon analysis to identify new key regulators. We identified six regulators that showed strong and positive correlation with iMES in the TCGA-KIRC cohort (all p < 0.001) including *EZH2* (r = 0.38), *KAT2A* (r = 0.20), *KDM5D* (r = 0.33), *KMT5A* (r = 0.31), *PRDM14* (r = 0.28), and *SIRT7* (r = 0.32) (Figure 6C and Table S14). Of note, *KMT5A* (r = 0.26, p = 0.053) and *EZH2* (r = 0.21, p = 0.098) were positively correlated with iMES in the BIONIKK ICI arms (Figure 6C and Table S14), consistent with the overexpression of *EZH2* in ccRCC tumors with epigenetic silencing. In addition, we found that iMES was inversely correlated with the regulon activity of *SETD2* (r = −0.24, p < 0.001) in the TCGA-KIRC cohort, indicating loss of *SETD2* for patients with high iMES, but there was no association in the BIONIKK cohort (Table S14). Nevertheless, we found that a *SETD2* loss signature was positively correlated with iMES (r = 0.26, p = 0.054) in the BIONIKK cohort as well as in the TCGA-KIRC cohort (r = 0.26, p < 0.001) (Figure 6C).

Moreover, *BAP1*-LCR signature was inversely correlated with iMES in both cohorts (r = −0.36, p < 0.0001 in TCGA-KIRC; r = −0.22, p = 0.084 in BIONIKK's ICI arms). We further explored the genes linked to the *BAP1*-loss-driven accessible chromatin regions, identifying a subset of these genes that were strongly and inversely correlated with iMES in both cohorts (Figure S11). These genes showed an enrichment in the hypoxia pathway (p = 0.021, FDR = 0.103), aligning with the observed endothelial cell depletion in tumors with low iMES. Conversely, a smaller set of genes displayed a positive correlation with iMES (Figure S11) and were enriched in proliferative pathways, including the G_2/M checkpoint and E2F targets (both p = 0.034, FDR = 0.135). These findings further substantiate the intricate interplay between epigenetic silencing, chromatin remodeling, and TME in shaping immunotherapy resistance in ccRCC.

iMES outperformed other transcriptomic signatures in predicting clinical resistance for Ipi/Nivo or nivolumab monotherapy

We then evaluated the prognostic relevance of published transcriptomic signatures in the BIONIKK and CheckMate cohorts,

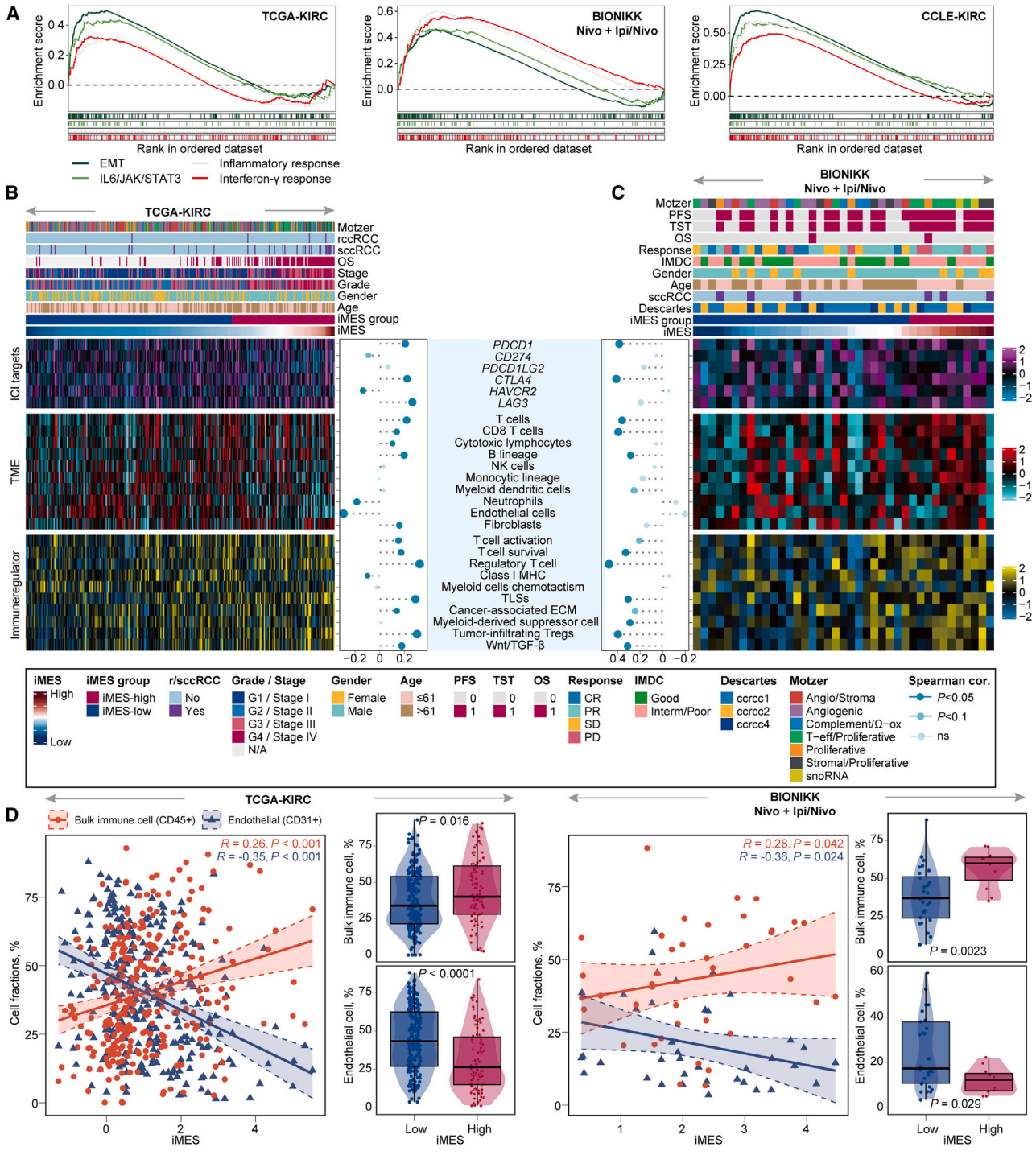

Figure 5. Biological relevance of iMES

(A) GSEA panels displaying activated Hallmark pathways in patients/cell lines with high iMES.

(B) TME landscape of TCGA cohort, with samples sorted in ascending order based on iMES. Dot plots, positioned alongside the heatmaps, display the correlation between iMES and the expression or enrichment levels of immune-related factors.

(C) Same as (B) but for BIONIKK's ICI arms.

(D) Association between iMES and cell fractions.

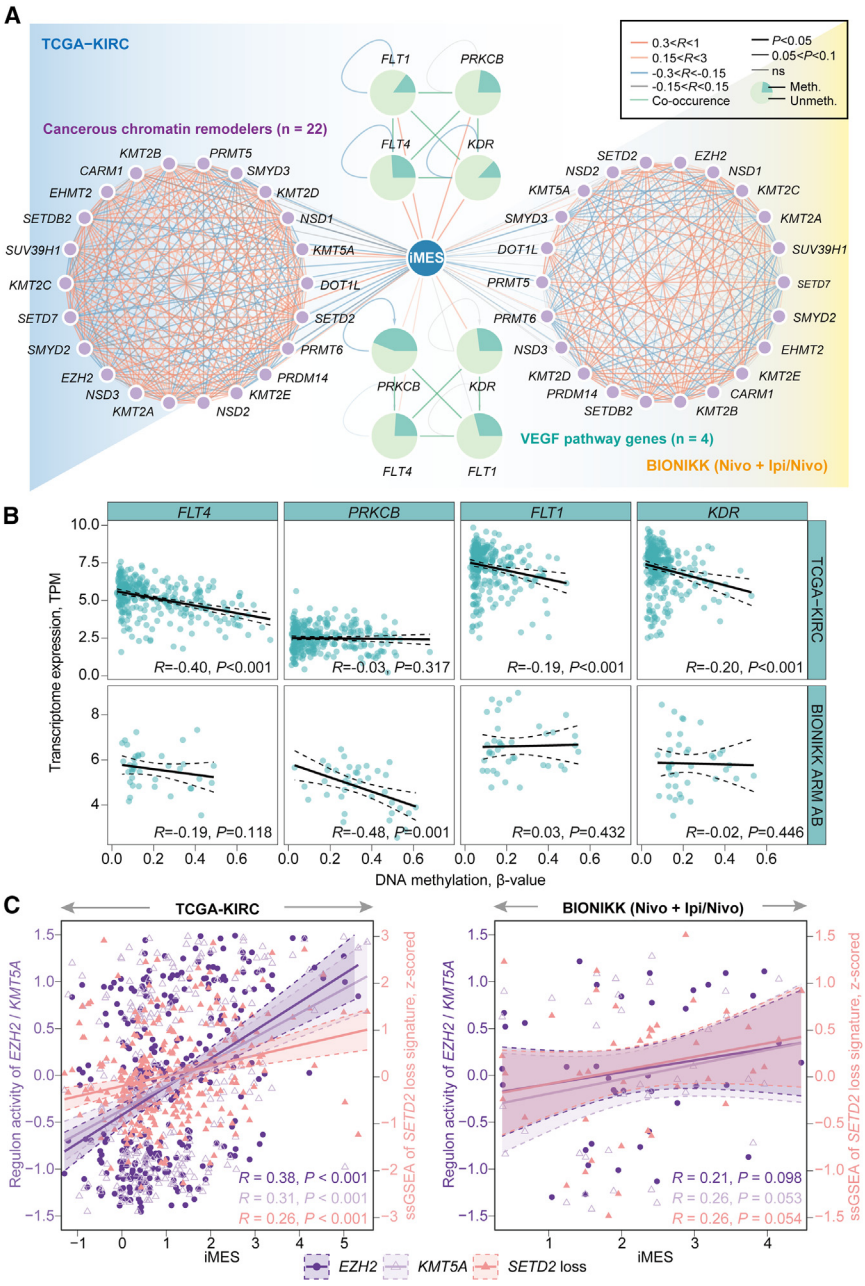

Figure 6. iMES association with VEGF and chromatin remodeling

(A) Network illustrating the association between iMES (blue dot) and methylation status of *VEGF* pathway genes (green pie chart), and regulon activity of cancerous chromatin remodelers (purple dots), as well as internal correlation among chromatin remodels, mutual exclusivity status of *VEGF* pathway genes (green lines connecting *VEGF* genes), and their self-correlation between gene-level DNA methylation and gene expression (directed bended lines around pie charts).

(B) Correlation between gene-level methylation and expression of the four *VEGF* pathway genes.

(C) Correlation between iMES and regulon activity of two chromatin remodelers (*EZH2* and *KMT5A*), and between iMES and single-sample GSEA score of *STED2* loss signature.

respectively. Four transcriptomic signatures that had previously been reported to be linked with ICI response were examined first: Teff, myeloid inflammation (Myeloid), Immuno, and tumor inflammation signature.[5,9,30] Of note, there was no statistical association between scores of these signatures with prognosis of patients receiving Ipi/Nivo or nivolumab monotherapy treatment (all p > 0.05; Table S15). As iMES was tightly associated with endothelial cells, which is essential for angiogenesis, we therefore investigated Angio, a transcriptomic angiogenesis signature previously reported to be linked with sunitinib response.[9] However, we found no statistical association between the Angio signature and clinical outcomes of patients receiving sunitinib in the BIONIKK or ccRCC-Descartes cohorts and also the patients who received everolimus in the CheckMate cohort (all p > 0.2; Table S15). Interestingly, we found a higher score of Angio signature was tightly associated with improved PFS (HR = 0.64, 95% CI 0.44–0.94, p = 0.022), TST (HR = 0.69, 95% CI 0.48–1.01, p = 0.055), and OS (HR = 0.31, 95% CI 0.17–0.57, p < 0.001) for patients in BIONIKK's ICI arms, and improved OS (HR = 0.80, 95% CI 0.69–0.92, p = 0.002) for patients in CheckMate's ICI arm (Table S15). These findings align with our earlier observation that silenced VEGF pathway genes and decreased endothelial cells correlate with ICI resistance.

In addition, for those 39 samples from the ICI arms that had both epigenetic and transcriptomic profiles, multivariate analyses demonstrated that iMES was an independent prognostic value when adjusting Angio signature scores with respect to PFS (HR = 1.76, 95% CI 1.14–2.72, p = 0.011) and TST (HR = 1.89, 95% CI 1.19–3.02, p = 0.007) (Table S16). This suggests that iMES offered insights beyond angiogenesis and also reflected other biological processes that could be important for tumor progression, as the endothelial cell enrichment and angiogenesis signature are related but not identical processes.

Translating epigenome-based iMES into a transcriptome-based analogous system

DNA methylation at the level of regulatory genes is associated with changes in the activity of the regulons they control, leading to a coordinated silencing of the genes within the regulon. Recognizing the limitation that some cohorts lack DNA

CellPress
OPEN ACCESS

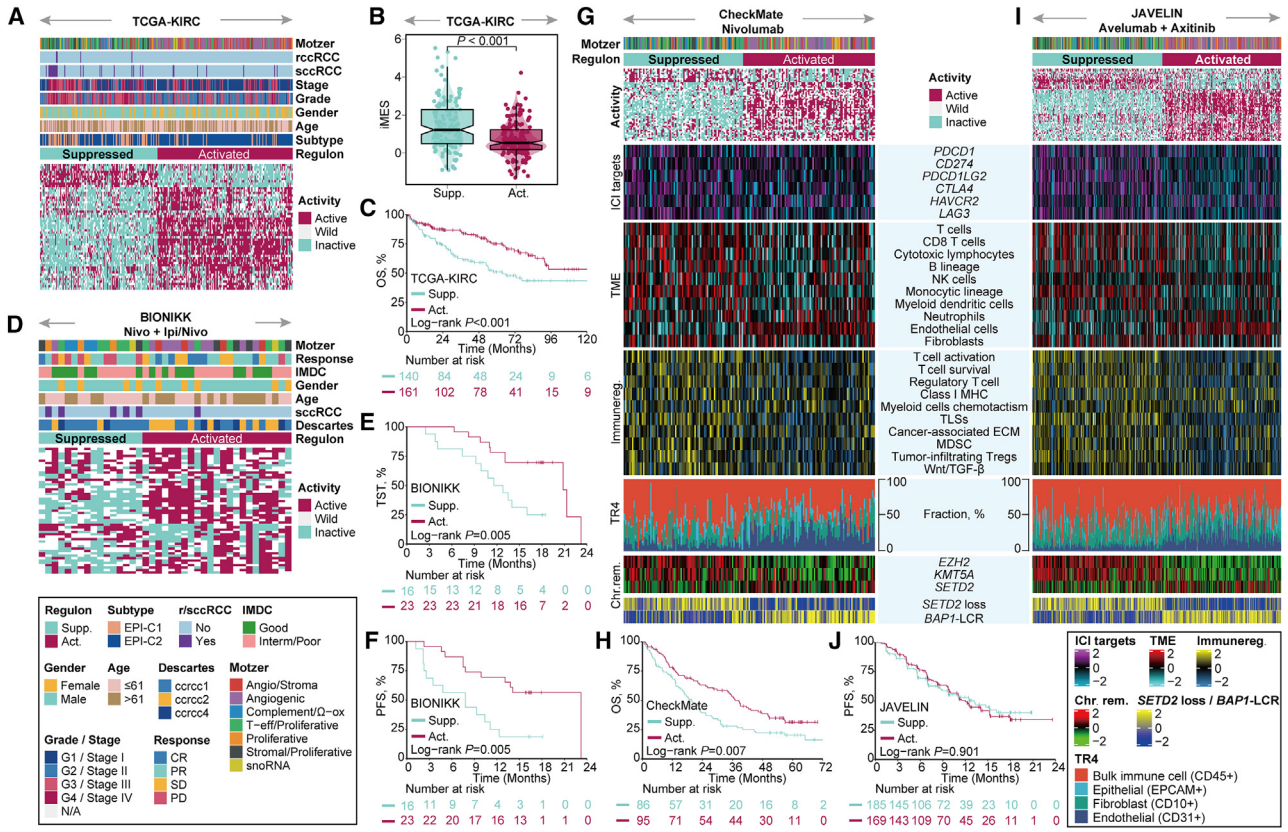

Figure 7. Regulon phenotypes and prognostic relevance in ccRCC

(A) *K*-mode clustering of genes corresponding to model-selected probes based on their regulon activity status in TCGA cohort.

(B) Violin plot of iMES between two regulon subtypes.

(C) Kaplan-Meier survival curves depicting OS rates of regulon subtypes in TCGA cohort.

(D) *K*-mode clustering using regulon activity status in BIONIKK's ICI arms.

(E) Kaplan-Meier curves differentiate TST of regulon subtypes in BIONIKK's ICI arms.

(F) Same as (E) but for PFS.

(G) *K*-mode clustering using regulon activity status (top panel), the TME landscape (middle panel) with deconvolution of cell fractions, and the regulon activity distribution of *EZH2*, *KMT5A*, and *SETD2* as well as the single-sample GSEA score of *SETD2* loss signature (bottom panel) in CheckMate's ICI arm.

(H) Kaplan-Meier survival curves depicting OS rates of regulon subtypes in CheckMate's ICI arm.

(I) Characterization of regulon phenotypes in JAVELIN's ICI/TKI arm.

(J) Kaplan-Meier survival curves depicting PFS rates of regulon subtypes in JAVELIN's ICI/TKI arm.

methylation data but possess RNA-seq profiles, we translated the epigenome-based iMES into a parallel system. This analogous system can utilize solely transcriptomic data for prognostic predictions in ccRCC patients undergoing ICI treatment.

The iMES is formulated on the promoter hypermethylation status of certain probes, a condition believed to induce gene silencing. However, the direct expression levels of these genes, as measured by RNA-seq, may not allow for an unambiguous determination of their functional activity within the transcriptional regulatory network. Instead it is the network-wide context, rather than individual gene expression, that yields a more precise representation of a gene's operational status within the cell (i.e., active or silenced). Therefore, we inferred the regulon activity status of the 54 genes corresponding to the probes constituting the iMES, reasoning that their collective activity status could mirror the iMES groups.

In the TCGA-KIRC cohort, we uncovered two distinct phenotypes exhibiting distinct regulon activity patterns (Figure 7A). The regulon-suppressed phenotype demonstrated a significantly higher iMES and was over-represented in patients in the iMES-high group compared to the regulon-activated phenotype (both $p < 0.001$; Figure 7B). As per the analogous system, a phenotype displaying a downregulated regulon pattern would signify a silenced state, similar to an iMES-high group. Conversely, a phenotype with an upregulated regulon pattern would suggest an active, non-silenced state, mirroring the iMES-low group. Survival analyses demonstrated significant prognostic relevance for OS, with the median survival being 63.7 months for the regulon-suppressed phenotype and not yet reached for the regulon-activated phenotype ($p < 0.001$; Figure 7C).

To further explore the prognostic capabilities of the analogous system in ccRCC patients undergoing ICI treatment, we

extended our analysis to the BIONIKK and CheckMate cohorts within which patients received Ipi/Nivo or nivolumab monotherapy. In these cohorts, two regulon phenotypes were triumphantly reproduced, with patients demonstrating the regulon-suppressed phenotype exhibiting significantly inferior prognoses compared to those within the regulon-activated phenotype.

In the BIONIKK ICI arms (Figure 7D), patients with the regulon-suppressed phenotype showed significantly shorter TST (median survival: regulon-suppressed = 12.2 months, regulon-activated = 20.8 months, p = 0.005) and PFS (median survival: regulon-suppressed = 7.8 months, regulon-activated = 23.2 months, p = 0.005) (Figures 7E and 7F) and a marginal enrichment of iMES-high patients (p = 0.076), while no statistical association was observed between regulon phenotype and iMES (p = 0.2).

In the CheckMate ICI arm (Figure 7G), the regulon-suppressed phenotype showed significantly poorer outcomes concerning OS (median survival: regulon-suppressed = 19.6 months, regulon-activated = 38.6 months, p = 0.007) (Figure 7H), and this phenotype was highly infiltrated by immune activation/suppressive populations but depleted for endothelial cells, which was consistent with the enrichment of angiogenic/stromal and angiogenic subtypes compared to the regulon-activated phenotype (62 [65%] vs. 10 [11.6%], p < 0.0001) (Figure 7G). Deconvolution analysis disclosed a higher proportion of immune cells but lower proportion of endothelial cells in the regulon-suppressed phenotype compared to the regulon-activated phenotype (both p < 0.001; Figure 7G). Likewise, the regulon phenotype in the CheckMate cohort tended to be an independent prognostic factor regarding OS when adjusting Angio signature scores (HR = 1.42, 95% CI 0.98–2.06, p = 0.067) (Table S16). The regulon-suppressed phenotype revealed significantly higher regulon activity of *EZH2* and *KMT5A* (both p < 0.001) and lower activity of *SETD2* (p = 0.017) (Table S17), which is consistent with a significantly higher level of *SETD2* loss signature (p < 0.001) compared to the regulon-activated phenotype (Figure 7G). Moreover, the regulon-suppressed phenotype was characterized by a significantly reduced level of the *BAP1*-LCR signature (p < 0.001), indicating *BAP1* loss in this phenotype.

In our exploration of the JAVELIN cohort within which patients were treated with a combination of ICI and TKI (avelumab + axitinib) that deviates from those in the BIONIKK and CheckMate cohorts, the two regulon phenotypes demonstrated a pattern similar to those previously observed (Figure 7I). The regulon-suppressed phenotype was characterized by increased immune infiltration, endothelial cell depletion, heightened activity of *EZH2* and *KMT5A*, and deficiency in *SETD2* and *BAP1* (Table S17). Similarly, we noted a significant enrichment of the angiogenic/stromal and angiogenic clusters within the regulon-activated phenotype (125 [74%] vs. 19 [10.3%], p < 0.0001). However, no statistical significance was discerned in terms of PFS between the phenotypes (p = 0.901; Figure 7J). This finding might introduce the possibility that these patients may respond to the ICI plus TKI treatment.

To evaluate the biological potential of the regulons, we conducted a meta-analysis across four ccRCC cohorts that identified 38 regulons with consistently inactive status in the regulon-suppressed phenotype in at least three cohorts, and no active regulons were identified for this phenotype (Table S18). Correlation analysis revealed enrichment of genes within these regulons in IL-6/JAK/STAT3 signaling (p = 0.032, FDR = 0.2) and inflammatory response pathways (p = 0.022, FDR = 0.17), highlighting their biological relevance in immune evasion (Table S19).

In subsequent investigations, we examined the potential prognostic and predictive value of regulon phenotypes. This involved an unsupervised analysis of transcriptome data from patients receiving sunitinib treatment in the BIONIKK (n = 9) and ccRCC-Descartes (n = 50) cohorts, along with patients under everolimus therapy in the CheckMate cohort (n = 130). Although two regulon phenotypes were identified in each cohort, no statistical significance was observed regarding prognosis for patients receiving sunitinib treatment in the BIONIKK (Figures S12A—S12C) and ccRCC-Descartes (Figures S12D—S12F) cohorts. Additionally, no prognostic association was inferred between regulon phenotypes and clinical outcomes for patients receiving everolimus therapy in the CheckMate cohort (Figures S12G and S12H). These findings suggested the potential prognostic and predictive value of the transcriptome-based regulon system that parallels the iMES.

DISCUSSION

Monoclonal antibodies targeting immune checkpoints have greatly improved outcomes for patients with advanced cancer, but a substantial proportion fail to respond, resulting in potential adverse reactions without positive response to the patients and poor cost-effectiveness to the healthcare system.[31] Discovery of reliable biomarkers that enable prediction of outcomes of ICI is therefore crucial, and emerging efforts have been made to achieve this, including the investigation of tumor mutation burden, PD-L1 expression, and transcriptome signatures. However, none of these have been validated across different cohorts or have shown benefit for front-line therapy in clinical settings.[32]

Our investigation delves into the synergistic potential of integrating DNA methylation and gene expression analysis, uncovering an epigenetically silenced ccRCC subgroup that exhibited primary resistance to immunotherapy in the BIONIKK trial. Notably, nearly a quarter of the silenced genes enriched in the chromosomal region 19q13.43 encode zinc-finger proteins, integral players in ccRCC progression and therapy resistance. This includes KRAB zinc-finger proteins (KRAB-ZFPs) such as *ZNF844* and *ZNF433*, located on chromosome 19, whose downregulation is associated with poor outcomes and immune evasion mechanisms exploited by aggressive tumors.[33–35] Furthermore, we introduced iMES as the only biomarker predictive of resistance to ICI in this trial. Patients with high iMES had specific TME features, including Treg enrichment and endothelial cell depletion, as well as activation of EMT and IL-6/JAK/STAT3 pathways, suggesting crosstalk between cancer cells and their associated immune and stromal ecosystems.

Differential methylation analyses revealed *PRC2* hypermethylation and *EZH2* overexpression in patients with high iMES. Intriguingly, these epigenetic alterations converge on *BAP1* loss, given the established link between *BAP1* loss and *EZH2* overexpression.[24] In uveal melanoma, *BAP1* loss is linked to the regulation or exclusion of T effector lymphocytes and the

polarization of macrophages toward a tolerogenic phenotype in the TME, thereby suppressing the immune system's ability to combat cancer cells.[36] In multiple cancers, elevated *EZH2* levels silence antigen presentation genes and tumor suppressors while driving Treg differentiation and immune suppression.[37,38] Accumulating evidence highlights *EZH2* as a pivotal factor in tumor immune resistance, advocating for its targeting in immunotherapy protocols.[28]

The close association between *SETD2* mutation or loss and epigenetic silencing in ccRCC did not emerge through abiogenesis, as *SETD2* mutation was significantly enriched in a clear-cell CpG island methylator phenotype that we identified previously based solely on the DNA methylation profile.[29] *SETD2* encodes for a histone methyltransferase that specifically targets histone 3, lysine 36 (H3K36), and *SETD2* is responsible for the trimethylation of H3K36 (H3K36me3), which is an epigenetic marker associated with active transcription and correct splicing. The loss of *SETD2* function in ccRCC leads to a decrease in H3K36me3 levels, resulting in mislocalization of DNA methyltransferases and further causing hypermethylation at normally unmethylated regions, such as gene promoters. This hypermethylation can trigger the transcriptional silencing of tumor-suppressor genes and the activation of oncogenes, ultimately contributing to tumor progression.[39,40] Here, we observed consistent *SETD2* loss in patients with high iMES or regulon-suppressed phenotypes, which might explain the aggressive phenotype characterized by cancer-specific hypermethylation-induced silencing. A recent study showed that *SETD2* deficiency in ccRCC may represent an attractive therapeutic vulnerability for DNA hypomethylating agents (HMAs), and further provided preclinical and *in vivo* evidence that *SETD2*-deficient tumors were extremely sensitive to combination treatment of HMAs and ICI.[41] Therefore, our convergent findings of *PRC2* hypermethylation, *EZH2* overexpression, and *BAP1* and *SETD2* loss provide valuable insights into the interplay between epigenetic alterations, immune modulation, and therapeutic implications in ccRCC patients who showed primary resistance to ICI treatment.

The BIONIKK trial yielded unexpected results in the pro-angiogenic ccrcc2 group, with a notably higher objective response rate of 51% among patients who received Ipi/Nivo. Moreover, the complete response rate was over 5-fold greater in this group for patients receiving Ipi/Nivo compared to those who received sunitinib, with rates of 16% and 3%, respectively.[19] Interestingly, patients with high iMES and primary resistance to ICI were also associated with epigenetic silencing of VEGF receptor genes. In addition, the Angio transcriptome signature was found to be effective in predicting clinical benefit of ccRCC patients from different cohorts receiving ICI. A successful active tumor immunotherapy requires not only activated tumor-antigen-specific T cells but also the access of T cells to malignant cells and an immune-supportive environment to sustain T cell function. In addition, sustained exposure to hypoxia has been shown to accelerate differentiation of $CD8^+$ T cells to terminal differentiation and dampens effective antitumor immunity.[42] These data are concordant with the results of the IMmotion 150 trial suggesting that angiogenesis signature is associated with improved response to sunitinib and atezolizumab plus bevacizumab.[5,9] Furthermore, a recent study indicated that patients with advanced melanoma who received anti-CTLA-4 therapy and experienced clinical benefit (i.e., achieved complete response or partial response) had a higher number of blood vessels compared to patients who did not respond to the therapy (i.e., had progressive disease).[43] As RNA-based biomarker studies have had limited success in identifying reliable biomarkers for immunotherapy response in ccRCC,[10,11] our findings provide additional evidence that a future model integrating iMES and the angiogenesis process or endothelial component might improve the prediction of response and prognosis of patients receiving immune checkpoint inhibitors in clinical settings.

Our exploration of the JAVELIN cohort brings forth intriguing possibilities. The high-iMES-paralleled regulon-suppressed patients with endothelial cell depletion responded to a treatment regimen involving a combination of ICI and TKI. This response occurred despite the presumed dependence of TKIs on endothelial cells for their anti-angiogenic effects, suggesting an alternative anti-proliferative mechanism.[44,45] Such nuanced findings underscore the importance of understanding tumor biology in shaping therapeutic strategies, especially when combining diverse agents.

Traditional RNA-based gene signatures face challenges in clinical application due to heterogeneity and technical biases across databases.[46–48] In contrast, iMES, grounded in binary methylation status, eliminates the need for intricate data normalization. This facilitates its clinical translation as an individualized survival estimator for ccRCC patients undergoing ICI therapy. High iMES could guide ICI-HMA/TKI combination treatments, while low iMES might favor Ipi/Nivo combination.

Despite facing challenges inherent in early-stage research, our study marks an important step toward understanding the role of epigenetic silencing in determining tumor aggressiveness and immune evasion in patients with ccRCC. In summary, the iMES offers a promising avenue for predicting primary resistance to ICI in ccRCC. Further investigations are warranted to corroborate these findings and determine their practicality in clinical contexts.

Limitations of the study

Limitations of the current study include the small sample size of the BIONIKK cohort, the limited cases with matched RNA-seq data, the need for studies at the single-cell level to confirm the association with an exhausted TME, and the paucity of materials available to see the changes of histone modifications (i.e., H3K36me3). Further limitation pertains to the use of univariate correlation analyses, which provide valuable insights into the direct relationships between variables of interest but do not account for potential confounding factors or interactions among variables. In addition, BIONIKK is currently the only clinical trial for immunotherapy with profiled DNA methylation data, which limits our ability to establish a universal iMES cutoff. As more diverse cohorts share methylation data, we will be able to refine and validate the iMES system for broader use.

STAR★METHODS

Detailed methods are provided in the online version of this paper and include the following:

- KEY RESOURCES TABLE
- RESOURCE AVAILABILITY

- Lead contact
- Materials availability
- Data and code availability

- EXPERIMENTAL MODEL AND STUDY PARTICIPANT DETAILS
  - Sample collection and ethical approval
- METHOD DETAILS
  - DNA methylation and RNA-sequencing profiling
  - RNA sequencing
  - Public DNA methylation 450K-array cohorts
  - DNA methylation and expression profiles for human renal cancer cell line
  - External RNA sequencing profile from clinical trials
- QUANTIFICATION AND STATISTICAL ANALYSIS
  - Quantification and filtering of DNA methylation profiles
  - Definition of promoters and cancer-specific hypermethylation
  - Epigenetic silencing calls
  - Identification of tumor-associated enhancer demethylator
  - Copy number variation analysis
  - Clustering analyses
  - Estimation of TME cell abundance and tumor purity
  - Chromatin remodeling and vascular endothelial growth factor signatures
  - Differential and enrichment analysis
  - Regulon analysis
  - Development of a DNA methylation-based epigenetic silencing index
  - Assessment of transcriptomic signatures
  - Classification of Motzer's seven molecular subtypes of ccRCC
  - Cell type fraction estimation
  - Statistical analyses

SUPPLEMENTAL INFORMATION

Supplemental information can be found online at https://doi.org/10.1016/j.xcrm.2023.101287.

ACKNOWLEDGMENTS

We would like to express our deepest gratitude to all the patients who participated in the clinical trials, the data from which were used in this study. We thank BioRender (BioRender.com) for providing the platform to create the graphical abstract and flow diagrams. This work was supported in part by grants from the Fondation ARC (SIGN'IT) (G.M.), Fondation AVEC (G.M.), National Natural Science Foundation of China (no. 81973145, no. 82273735) (F.Y.), and Key R&D Program of Jiangsu Province (Social Development) (BE2020694) (F.Y.).

AUTHOR CONTRIBUTIONS

Conceptualization, X.L., Y.-A.V., S.O., and G.G.M.; methodology, X.L., X.S., W.C., L.X., and G.G.M.; data collection, Y.-A.V., A.H., V.L., R.M., J.-P.S., M.R., E.C., V.V., C.-M.S., M.B., H.L., P.B., W.H.F., C.S.-F., S.O., and G.G.M.; investigation, all authors; bioinformatics analysis, X.L. and X.S.; statistical analysis, X.L., W.C., L.X., and F.Y.; software, X.L.; data interpretation, X.L., Y.-A.V., X.S., C.-M.S., W.H.F., C.S.-F., S.O., and G.G.M., writing – original draft, all authors; writing – review & editing, X.L., Y.-A.V., X.S., I.D., S.O., and G.G.M.; funding acquisition, F.Y. and G.G.M.; supervision, S.O. and G.G.M.

DECLARATION OF INTERESTS

The authors declare no competing interests.

Received: May 8, 2023
Revised: July 21, 2023
Accepted: October 19, 2023
Published: November 14, 2023

REFERENCES

1. Jonasch, E., Walker, C.L., and Rathmell, W.K. (2021). Clear cell renal cell carcinoma ontogeny and mechanisms of lethality. Nat. Rev. Nephrol. *17*, 245–261. https://doi.org/10.1038/s41581-020-00359-2.
2. Hsieh, J.J., Purdue, M.P., Signoretti, S., Swanton, C., Albiges, L., Schmidinger, M., Heng, D.Y., Larkin, J., and Ficarra, V. (2017). Renal cell carcinoma. Nat. Rev. Dis. Prim. *3*, 17009. https://doi.org/10.1038/nrdp.2017.9.
3. Motzer, R.J., Jonasch, E., Boyle, S., Carlo, M.I., Manley, B., Agarwal, N., Alva, A., Beckermann, K., Choueiri, T.K., Costello, B.A., et al. (2020). NCCN Guidelines Insights: Kidney Cancer, Version 1.2021. J. Natl. Compr. Cancer Netw. *18*, 1160–1170. https://doi.org/10.6004/jnccn.2020.0043.
4. Motzer, R.J., Tannir, N.M., McDermott, D.F., Arén Frontera, O., Melichar, B., Choueiri, T.K., Plimack, E.R., Barthélémy, P., Porta, C., George, S., et al. (2018). Nivolumab plus Ipilimumab versus Sunitinib in Advanced Renal-Cell Carcinoma. N. Engl. J. Med. *378*, 1277–1290. https://doi.org/10.1056/NEJMoa1712126.
5. Motzer, R.J., Robbins, P.B., Powles, T., Albiges, L., Haanen, J.B., Larkin, J., Mu, X.J., Ching, K.A., Uemura, M., Pal, S.K., et al. (2020). Avelumab plus axitinib versus sunitinib in advanced renal cell carcinoma: biomarker analysis of the phase 3 JAVELIN Renal 101 trial. Nat. Med. *26*, 1733–1741. https://doi.org/10.1038/s41591-020-1044-8.
6. Motzer, R.J., Banchereau, R., Hamidi, H., Powles, T., McDermott, D., Atkins, M.B., Escudier, B., Liu, L.F., Leng, N., Abbas, A.R., et al. (2020). Molecular Subsets in Renal Cancer Determine Outcome to Checkpoint and Angiogenesis Blockade. Cancer Cell *38*, 803–817.e4. https://doi.org/10.1016/j.ccell.2020.10.011.
7. Pourmir, I., Noel, J., Simonaggio, A., Oudard, S., and Vano, Y.A. (2021). Update on the most promising biomarkers of response to immune checkpoint inhibitors in clear cell renal cell carcinoma. World J. Urol. *39*, 1377–1385. https://doi.org/10.1007/s00345-020-03528-x.
8. Krishna, C., DiNatale, R.G., Kuo, F., Srivastava, R.M., Vuong, L., Chowell, D., Gupta, S., Vanderbilt, C., Purohit, T.A., Liu, M., et al. (2021). Single-cell sequencing links multiregional immune landscapes and tissue-resident T cells in ccRCC to tumor topology and therapy efficacy. Cancer Cell *39*, 662–677.e6. https://doi.org/10.1016/j.ccell.2021.03.007.
9. McDermott, D.F., Huseni, M.A., Atkins, M.B., Motzer, R.J., Rini, B.I., Escudier, B., Fong, L., Joseph, R.W., Pal, S.K., Reeves, J.A., et al. (2018). Clinical activity and molecular correlates of response to atezolizumab alone or in combination with bevacizumab versus sunitinib in renal cell carcinoma. Nat. Med. *24*, 749–757. https://doi.org/10.1038/s41591-018-0053-3.
10. Motzer, R.J., Choueiri, T.K., McDermott, D.F., Powles, T., Yao, J., Ammar, R., Papillon-Cavanagh, S., Saggi, S.S., McHenry, B.M., Ross-Macdonald, P., and Wind-Rotolo, M. (2020). Biomarker analyses from the phase III CheckMate 214 trial of nivolumab plus ipilimumab (N+I) or sunitinib (S) in advanced renal cell carcinoma (aRCC). J. Clin. Oncol. *38*, 5009. https://doi.org/10.1200/JCO.2020.38.15_suppl.5009.
11. Braun, D.A., Hou, Y., Bakouny, Z., Ficial, M., Sant' Angelo, M., Forman, J., Ross-Macdonald, P., Berger, A.C., Jegede, O.A., Elagina, L., et al. (2020). Interplay of somatic alterations and immune infiltration modulates response to PD-1 blockade in advanced clear cell renal cell carcinoma. Nat. Med. *26*, 909–918. https://doi.org/10.1038/s41591-020-0839-y.

12. Lu, X., Vano, Y., Helleux, A., Su, X., Lindner, V., Davidson, G., Mouawad, R., Spano, J.-P., Rouprêt, M., Elaidi, R., et al. (2023). An enhancer demethylator phenotype converged to immune dysfunction and resistance to immune checkpoint inhibitors in clear-cell renal cell carcinomas. Clin. Cancer Res. *29*, 1279–1291. https://doi.org/10.1158/1078-0432.Ccr-22-2133.

13. Zhou, M., and Kim, W.Y. (2023). Viewing RCC with a DNA Methylation Lens ENHANCES Understanding of ICI Resistance (Clinical Cancer Research), OF1-OF3. https://doi.org/10.1158/1078-0432.Ccr-22-3574.

14. Nabais, M.F., Gadd, D.A., Hannon, E., Mill, J., McRae, A.F., and Wray, N.R. (2023). An overview of DNA methylation-derived trait score methods and applications. Genome Biol. *24*, 28. https://doi.org/10.1186/s13059-023-02855-7.

15. Shirley, M. (2020). Epi proColon(®) for Colorectal Cancer Screening: A Profile of Its Use in the USA. Mol. Diagn. Ther. *24*, 497–503. https://doi.org/10.1007/s40291-020-00473-8.

16. Wise, J. (2022). A blood test for multiple cancers: game changer or overhyped? Br. Med. J. *378*, o2279. https://doi.org/10.1136/bmj.o2279.

17. Horvath, S., Gurven, M., Levine, M.E., Trumble, B.C., Kaplan, H., Allayee, H., Ritz, B.R., Chen, B., Lu, A.T., Rickabaugh, T.M., et al. (2016). An epigenetic clock analysis of race/ethnicity, sex, and coronary heart disease. Genome Biol. *17*, 171. https://doi.org/10.1186/s13059-016-1030-0.

18. Beuselinck, B., Job, S., Becht, E., Karadimou, A., Verkarre, V., Couchy, G., Giraldo, N., Rioux-Leclercq, N., Molinié, V., Sibony, M., et al. (2015). Molecular Subtypes of Clear Cell Renal Cell Carcinoma Are Associated with Sunitinib Response in the Metastatic Setting. Clin. Cancer Res. *21*, 1329–1339. https://doi.org/10.1158/1078-0432.Ccr-14-1128.

19. Vano, Y.-A., Elaidi, R., Bennamoun, M., Chevreau, C., Borchiellini, D., Pannier, D., Maillet, D., Gross-Goupil, M., Tournigand, C., Laguerre, B., et al. (2022). Nivolumab, nivolumab–ipilimumab, and VEGFR-tyrosine kinase inhibitors as first-line treatment for metastatic clear-cell renal cell carcinoma (BIONIKK): a biomarker-driven, open-label, non-comparative, randomised, phase 2 trial. Lancet Oncol. https://doi.org/10.1016/S1470-2045(22)00128-0.

20. Malouf, G.G., Ali, S.M., Wang, K., Balasubramanian, S., Ross, J.S., Miller, V.A., Stephens, P.J., Khayat, D., Pal, S.K., Su, X., et al. (2016). Genomic Characterization of Renal Cell Carcinoma with Sarcomatoid Dedifferentiation Pinpoints Recurrent Genomic Alterations. Eur. Urol. *70*, 348–357. https://doi.org/10.1016/j.eururo.2016.01.051.

21. Bakouny, Z., Braun, D.A., Shukla, S.A., Pan, W., Gao, X., Hou, Y., Flaifel, A., Tang, S., Bosma-Moody, A., He, M.X., et al. (2021). Integrative molecular characterization of sarcomatoid and rhabdoid renal cell carcinoma. Nat. Commun. *12*, 808. https://doi.org/10.1038/s41467-021-21068-9.

22. El-Mokadem, I., Fitzpatrick, J., Rai, B., Cunningham, J., Pratt, N., Fleming, S., and Nabi, G. (2014). Significance of Chromosome 9p Status in Renal Cell Carcinoma: A Systematic Review and Quality of the Reported Studies. BioMed Res. Int. *2014*, 521380. https://doi.org/10.1155/2014/521380.

23. Wei, J.H., Haddad, A., Wu, K.J., Zhao, H.W., Kapur, P., Zhang, Z.L., Zhao, L.Y., Chen, Z.H., Zhou, Y.Y., Zhou, J.C., et al. (2015). A CpG-methylation-based assay to predict survival in clear cell renal cell carcinoma. Nat. Commun. *6*, 8699. https://doi.org/10.1038/ncomms9699.

24. LaFave, L.M., Béguelin, W., Koche, R., Teater, M., Spitzer, B., Chramiec, A., Papalexi, E., Keller, M.D., Hricik, T., Konstantinoff, K., et al. (2015). Loss of BAP1 function leads to EZH2-dependent transformation. Nat. Med. *21*, 1344–1349. https://doi.org/10.1038/nm.3947.

25. Wu, Y., Terekhanova, N.V., Caravan, W., Naser Al Deen, N., Lal, P., Chen, S., Mo, C.-K., Cao, S., Li, Y., Karpova, A., et al. (2023). Epigenetic and transcriptomic characterization reveals progression markers and essential pathways in clear cell renal cell carcinoma. Nat. Commun. *14*, 1681. https://doi.org/10.1038/s41467-023-37211-7.

26. Johnson, D.E., O'Keefe, R.A., and Grandis, J.R. (2018). Targeting the IL-6/JAK/STAT3 signalling axis in cancer. Nat. Rev. Clin. Oncol. *15*, 234–248. https://doi.org/10.1038/nrclinonc.2018.8.

27. Jiang, P., Gu, S., Pan, D., Fu, J., Sahu, A., Hu, X., Li, Z., Traugh, N., Bu, X., Li, B., et al. (2018). Signatures of T cell dysfunction and exclusion predict cancer immunotherapy response. Nat. Med. *24*, 1550–1558.

28. Emran, A.A., Chatterjee, A., Rodger, E.J., Tiffen, J.C., Gallagher, S.J., Eccles, M.R., and Hersey, P. (2019). Targeting DNA Methylation and EZH2 Activity to Overcome Melanoma Resistance to Immunotherapy. Trends Immunol. *40*, 328–344. https://doi.org/10.1016/j.it.2019.02.004.

29. Su, X., Zhang, J., Mouawad, R., Compérat, E., Rouprêt, M., Allanic, F., Parra, J., Bitker, M.O., Thompson, E.J., Gowrishankar, B., et al. (2017). NSD1 Inactivation and SETD2 Mutation Drive a Convergence toward Loss of Function of H3K36 Writers in Clear Cell Renal Cell Carcinomas. Cancer Res. *77*, 4835–4845. https://doi.org/10.1158/0008-5472.Can-17-0143.

30. Danaher, P., Warren, S., Lu, R., Samayoa, J., Sullivan, A., Pekker, I., Wallden, B., Marincola, F.M., and Cesano, A. (2018). Pan-cancer adaptive immune resistance as defined by the Tumor Inflammation Signature (TIS): results from The Cancer Genome Atlas (TCGA). J. Immunother. Cancer *6*, 63. https://doi.org/10.1186/s40425-018-0367-1.

31. Sharma, P., Hu-Lieskovan, S., Wargo, J.A., and Ribas, A. (2017). Primary, Adaptive, and Acquired Resistance to Cancer Immunotherapy. Cell *168*, 707–723. https://doi.org/10.1016/j.cell.2017.01.017.

32. Rini, B.I., Brugarolas, J., and Atkins, M.B. (2023). Navigating and adapting care integrating immunotherapy, antiangiogenic therapy, and combinations in patients with advanced renal cell carcinoma. J. Immunother. Cancer *11*, e006361. https://doi.org/10.1136/jitc-2022-006361.

33. Cassandri, M., Smirnov, A., Novelli, F., Pitolli, C., Agostini, M., Malewicz, M., Melino, G., and Raschellà, G. (2017). Zinc-finger proteins in health and disease. Cell Death Dis. *3*, 17071. https://doi.org/10.1038/cddiscovery.2017.71.

34. Heyliger, S.O., Soliman, K.F.A., Saulsbury, M.D., and Reams, R.R. (2021). The Identification of Zinc-Finger Protein 433 as a Possible Prognostic Biomarker for Clear-Cell Renal Cell Carcinoma. Biomolecules *11*, 1193.

35. Heyliger, S.O., Soliman, K.F.A., Saulsbury, M.D., and Reams, R.R. (2022). Prognostic Relevance of ZNF844 and Chr 19p13.2 KRAB-Zinc Finger Proteins in Clear Cell Renal Carcinoma. Cancer Genomics Proteomics *19*, 305–327. https://doi.org/10.21873/cgp.20322.

36. Figueiredo, C.R., Kalirai, H., Sacco, J.J., Azevedo, R.A., Duckworth, A., Slupsky, J.R., Coulson, J.M., and Coupland, S.E. (2020). Loss of BAP1 expression is associated with an immunosuppressive microenvironment in uveal melanoma, with implications for immunotherapy development. J. Pathol. *250*, 420–439. https://doi.org/10.1002/path.5384.

37. Zingg, D., Arenas-Ramirez, N., Sahin, D., Rosalia, R.A., Antunes, A.T., Haeusel, J., Sommer, L., and Boyman, O. (2017). The Histone Methyltransferase Ezh2 Controls Mechanisms of Adaptive Resistance to Tumor Immunotherapy. Cell Rep. *20*, 854–867. https://doi.org/10.1016/j.celrep.2017.07.007.

38. Wang, D., Quiros, J., Mahuron, K., Pai, C.C., Ranzani, V., Young, A., Silveria, S., Harwin, T., Abnousian, A., Pagani, M., et al. (2018). Targeting EZH2 Reprograms Intratumoral Regulatory T Cells to Enhance Cancer Immunity. Cell Rep. *23*, 3262–3274. https://doi.org/10.1016/j.celrep.2018.05.050.

39. Tiedemann, R.L., Hlady, R.A., Hanavan, P.D., Lake, D.F., Tibes, R., Lee, J.-H., Choi, J.-H., Ho, T.H., and Robertson, K.D. (2016). Dynamic reprogramming of DNA methylation in SETD2-deregulated renal cell carcinoma. Oncotarget *7*, 1927–1946.

40. Xie, Y., Sahin, M., Sinha, S., Wang, Y., Nargund, A.M., Lyu, Y., Han, S., Dong, Y., Hsieh, J.J., Leslie, C.S., and Cheng, E.H. (2022). SETD2 loss perturbs the kidney cancer epigenetic landscape to promote metastasis and engenders actionable dependencies on histone chaperone complexes. Nat. Can. (Ott.) *3*, 188–202. https://doi.org/10.1038/s43018-021-00316-3.

41. Li, H.-T., Jang, H.J., Rohena-Rivera, K., Liu, M., Gujar, H., Kulchycki, J., Zhao, S., Billet, S., Zhou, X., Weisenberger, D.J., et al. (2023). RNA mis-splicing drives viral mimicry response after DNMTi therapy in

SETD2-mutant kidney cancer. Cell Rep. *42*, 112016. https://doi.org/10.1016/j.celrep.2023.112016.

42. Scharping, N.E., Rivadeneira, D.B., Menk, A.V., Vignali, P.D.A., Ford, B.R., Rittenhouse, N.L., Peralta, R., Wang, Y., Wang, Y., DePeaux, K., et al. (2021). Mitochondrial stress induced by continuous stimulation under hypoxia rapidly drives T cell exhaustion. Nat. Immunol. *22*, 205–215. https://doi.org/10.1038/s41590-020-00834-9.

43. Campbell, K.M., Amouzgar, M., Pfeiffer, S.M., Howes, T.R., Medina, E., Travers, M., Steiner, G., Weber, J.S., Wolchok, J.D., Larkin, J., et al. (2023). Prior anti-CTLA-4 therapy impacts molecular characteristics associated with anti-PD-1 response in advanced melanoma. Cancer Cell *41*, 791–806.e4. https://doi.org/10.1016/j.ccell.2023.03.010.

44. Canter, R.J., Ames, E., Mac, S., Grossenbacher, S.K., Chen, M., Li, C.S., Borys, D., Smith, R.C., Tellez, J., Sayers, T.J., et al. (2014). Anti-proliferative but not anti-angiogenic tyrosine kinase inhibitors enrich for cancer stem cells in soft tissue sarcoma. BMC Cancer *14*, 756. https://doi.org/10.1186/1471-2407-14-756.

45. Zhang, Y., Xue, D., Wang, X., Lu, M., Gao, B., and Qiao, X. (2014). Screening of kinase inhibitors targeting BRAF for regulating autophagy based on kinase pathways. Mol. Med. Rep. *9*, 83–90. https://doi.org/10.3892/mmr.2013.1781.

46. Patil, P., Bachant-Winner, P.-O., Haibe-Kains, B., and Leek, J.T. (2015). Test set bias affects reproducibility of gene signatures. Bioinformatics *31*, 2318–2323.

47. Walsh, C.J., Hu, P., Batt, J., and Santos, C.C.D. (2015). Microarray meta-analysis and cross-platform normalization: integrative genomics for robust biomarker discovery. Microarrays *4*, 389–406.

48. Leek, J.T., Scharpf, R.B., Bravo, H.C., Simcha, D., Langmead, B., Johnson, W.E., Geman, D., Baggerly, K., and Irizarry, R.A. (2010). Tackling the widespread and critical impact of batch effects in high-throughput data. Nat. Rev. Genet. *11*, 733–739.

49. Cancer Genome Atlas Research Network (2013). Comprehensive molecular characterization of clear cell renal cell carcinoma. Nature *499*, 43–49. https://doi.org/10.1038/nature12222.

50. Iorio, F., Knijnenburg, T.A., Vis, D.J., Bignell, G.R., Menden, M.P., Schubert, M., Aben, N., Gonçalves, E., Barthorpe, S., Lightfoot, H., et al. (2016). A Landscape of Pharmacogenomic Interactions in Cancer. Cell *166*, 740–754. https://doi.org/10.1016/j.cell.2016.06.017.

51. Dobin, A., Davis, C.A., Schlesinger, F., Drenkow, J., Zaleski, C., Jha, S., Batut, P., Chaisson, M., and Gingeras, T.R. (2013). STAR: ultrafast universal RNA-seq aligner. Bioinformatics *29*, 15–21. https://doi.org/10.1093/bioinformatics/bts635.

52. Colaprico, A., Silva, T.C., Olsen, C., Garofano, L., Cava, C., Garolini, D., Sabedot, T.S., Malta, T.M., Pagnotta, S.M., Castiglioni, I., et al. (2016). TCGAbiolinks: an R/Bioconductor package for integrative analysis of TCGA data. Nucleic Acids Res. *44*, e71. https://doi.org/10.1093/nar/gkv1507.

53. Tian, Y., Morris, T.J., Webster, A.P., Yang, Z., Beck, S., Feber, A., and Teschendorff, A.E. (2017). ChAMP: updated methylation analysis pipeline for Illumina BeadChips. Bioinformatics *33*, 3982–3984. https://doi.org/10.1093/bioinformatics/btx513.

54. Becht, E., Giraldo, N.A., Lacroix, L., Buttard, B., Elarouci, N., Petitprez, F., Selves, J., Laurent-Puig, P., Sautès-Fridman, C., Fridman, W.H., and de Reyniès, A. (2016). Estimating the population abundance of tissue-infiltrating immune and stromal cell populations using gene expression. Genome Biol. *17*, 218. https://doi.org/10.1186/s13059-016-1070-5.

55. Barbie, D.A., Tamayo, P., Boehm, J.S., Kim, S.Y., Moody, S.E., Dunn, I.F., Schinzel, A.C., Sandy, P., Meylan, E., Scholl, C., et al. (2009). Systematic RNA interference reveals that oncogenic KRAS-driven cancers require TBK1. Nature *462*, 108–112.

56. Peters, T.J., Buckley, M.J., Statham, A.L., Pidsley, R., Samaras, K., V Lord, R., Clark, S.J., and Molloy, P.L. (2015). De novo identification of differentially methylated regions in the human genome. Epigenet. Chromatin *8*, 6. https://doi.org/10.1186/1756-8935-8-6.

57. Phipson, B., Maksimovic, J., and Oshlack, A. (2016). missMethyl: an R package for analyzing data from Illumina's HumanMethylation450 platform. Bioinformatics *32*, 286–288. https://doi.org/10.1093/bioinformatics/btv560.

58. Ritchie, M.E., Phipson, B., Wu, D., Hu, Y., Law, C.W., Shi, W., and Smyth, G.K. (2015). limma powers differential expression analyses for RNA-sequencing and microarray studies. Nucleic Acids Res. *43*, e47. https://doi.org/10.1093/nar/gkv007.

59. Lu, X., Meng, J., Zhou, Y., Jiang, L., and Yan, F. (2021). MOVICS: an R package for multi-omics integration and visualization in cancer subtyping. Bioinformatics *36*, 5539–5541. https://doi.org/10.1093/bioinformatics/btaa1018.

60. Wu, T., Hu, E., Xu, S., Chen, M., Guo, P., Dai, Z., Feng, T., Zhou, L., Tang, W., Zhan, L., et al. (2021). clusterProfiler 4.0: A universal enrichment tool for interpreting omics data. Innovation *2*, 100141. https://doi.org/10.1016/j.xinn.2021.100141.

61. Castro, M.A.A., de Santiago, I., Campbell, T.M., Vaughn, C., Hickey, T.E., Ross, E., Tilley, W.D., Markowetz, F., Ponder, B.A.J., and Meyer, K.B. (2016). Regulators of genetic risk of breast cancer identified by integrative network analysis. Nat. Genet. *48*, 12–21. https://doi.org/10.1038/ng.3458.

62. Liu, B., Yang, X., Wang, T., Lin, J., Kang, Y., Jia, P., and Ye, K. (2019). MEpurity: estimating tumor purity using DNA methylation data. Bioinformatics *35*, 5298–5300. https://doi.org/10.1093/bioinformatics/btz555.

63. Mermel, C.H., Schumacher, S.E., Hill, B., Meyerson, M.L., Beroukhim, R., and Getz, G. (2011). GISTIC2.0 facilitates sensitive and confident localization of the targets of focal somatic copy-number alteration in human cancers. Genome Biol. *12*, R41. https://doi.org/10.1186/gb-2011-12-4-r41.

64. Sherman, B.T., Hao, M., Qiu, J., Jiao, X., Baseler, M.W., Lane, H.C., Imamichi, T., and Chang, W. (2022). DAVID: a web server for functional enrichment analysis and functional annotation of gene lists (2021 update). Nucleic Acids Res. *50*, W216–W221. https://doi.org/10.1093/nar/gkac194.

65. Xie, Z., Bailey, A., Kuleshov, M.V., Clarke, D.J.B., Evangelista, J.E., Jenkins, S.L., Lachmann, A., Wojciechowicz, M.L., Kropiwnicki, E., Jagodnik, K.M., et al. (2021). Gene Set Knowledge Discovery with Enrichr. Curr. Protoc. *1*, e90. https://doi.org/10.1002/cpz1.90.

66. Hoshida, Y. (2010). Nearest template prediction: a single-sample-based flexible class prediction with confidence assessment. PLoS One *5*, e15543. https://doi.org/10.1371/journal.pone.0015543.

67. Newman, A.M., Steen, C.B., Liu, C.L., Gentles, A.J., Chaudhuri, A.A., Scherer, F., Khodadoust, M.S., Esfahani, M.S., Luca, B.A., Steiner, D., et al. (2019). Determining cell type abundance and expression from bulk tissues with digital cytometry. Nat. Biotechnol. *37*, 773–782. https://doi.org/10.1038/s41587-019-0114-2.

68. Harrow, J., Frankish, A., Gonzalez, J.M., Tapanari, E., Diekhans, M., Kokocinski, F., Aken, B.L., Barrell, D., Zadissa, A., Searle, S., et al. (2012). GENCODE: the reference human genome annotation for The ENCODE Project. Genome Res. *22*, 1760–1774. https://doi.org/10.1101/gr.135350.111.

69. Liberzon, A., Subramanian, A., Pinchback, R., Thorvaldsdóttir, H., Tamayo, P., and Mesirov, J.P. (2011). Molecular signatures database (MSigDB) 3.0. Bioinformatics *27*, 1739–1740. https://doi.org/10.1093/bioinformatics/btr260.

70. Nishimura, D. (2001). BioCarta. Biotech Software & Internet Report. The Computer Software Journal for Scient *2*, 117–120.

71. Luca, B.A., Steen, C.B., Matusiak, M., Azizi, A., Varma, S., Zhu, C., Przybyl, J., Espín-Pérez, A., Diehn, M., Alizadeh, A.A., et al. (2021). Atlas of clinically distinct cell states and ecosystems across human solid tumors. Cell *184*, 5482–5496.e28. https://doi.org/10.1016/j.cell.2021.09.014.

72. Davidson, G., Helleux, A., Vano, Y.A., Lindner, V., Fattori, A., Cerciat, M., Elaidi, R.T., Verkarre, V., Sun, C.-M., Chevreau, C., et al. (2023). Mesenchymal-like tumor cells and myofibroblastic cancer-associated fibroblasts

are associated with progression and immunotherapy response of clear-cell renal cell carcinoma. Cancer Res. *83*, 2952–2969. https://doi.org/10.1158/0008-5472.Can-22-3034.

73. Malouf, G.G., Zhang, J., Yuan, Y., Compérat, E., Rouprêt, M., Cussenot, O., Chen, Y., Thompson, E.J., Tannir, N.M., Weinstein, J.N., et al. (2015). Characterization of long non-coding RNA transcriptome in clear-cell renal cell carcinoma by next-generation deep sequencing. Mol. Oncol. *9*, 32–43. https://doi.org/10.1016/j.molonc.2014.07.007.
74. Ghandi, M., Huang, F.W., Jané-Valbuena, J., Kryukov, G.V., Lo, C.C., McDonald, E.R., 3rd, Barretina, J., Gelfand, E.T., Bielski, C.M., Li, H., et al. (2019). Next-generation characterization of the Cancer Cell Line Encyclopedia. Nature *569*, 503–508. https://doi.org/10.1038/s41586-019-1186-3.
75. Zhou, W., Laird, P.W., and Shen, H. (2017). Comprehensive characterization, annotation and innovative use of Infinium DNA methylation BeadChip probes. Nucleic Acids Res. *45*, e22. https://doi.org/10.1093/nar/gkw967.
76. Feber, A., Guilhamon, P., Lechner, M., Fenton, T., Wilson, G.A., Thirlwell, C., Morris, T.J., Flanagan, A.M., Teschendorff, A.E., Kelly, J.D., and Beck, S. (2014). Using high-density DNA methylation arrays to profile copy number alterations. Genome Biol. *15*, R30. https://doi.org/10.1186/gb-2014-15-2-r30.
77. Meng, J., Zhou, Y., Lu, X., Bian, Z., Chen, Y., Zhou, J., Zhang, L., Hao, Z., Zhang, M., and Liang, C. (2021). Immune response drives outcomes in prostate cancer: implications for immunotherapy. Mol. Oncol. *15*, 1358–1375. https://doi.org/10.1002/1878-0261.12887.
78. Audia, J.E., and Campbell, R.M. (2016). Histone Modifications and Cancer. Cold Spring Harbor Perspect. Biol. *8*, a019521. https://doi.org/10.1101/cshperspect.a019521.
79. Lu, X., Meng, J., Su, L., Jiang, L., Wang, H., Zhu, J., Huang, M., Cheng, W., Xu, L., Ruan, X., et al. (2021). Multi-omics consensus ensemble refines the classification of muscle-invasive bladder cancer with stratified prognosis, tumour microenvironment and distinct sensitivity to frontline therapies. Clin. Transl. Med. *11*, e601. https://doi.org/10.1002/ctm2.601.
80. Ritchie, M.E., Phipson, B., Wu, D., Hu, Y., Law, C.W., Shi, W., and Smyth, G.K. (2015). limma powers differential expression analyses for RNA-sequencing and microarray studies. Nucleic Acids Res. *43*, e47.
81. Zou, H. (2006). The adaptive lasso and its oracle properties. J. Am. Stat. Assoc. *101*, 1418–1429.
82. Lu, X., Meng, J., Zhu, J., Zhou, Y., Jiang, L., Wang, Y., Wen, W., Liang, C., and Yan, F. (2021). Prognosis stratification and personalized treatment in bladder cancer through a robust immune gene pair-based signature. Clin. Transl. Med. *11*, e453. https://doi.org/10.1002/ctm2.453.
83. Lu, X., Tawanaie Pour Sedehi, N., Su, X., Yan, F., Alhalabi, O., Tannir, N.M., and Malouf, G.G. (2023). Racial Disparities in MiT Family Translocation Renal Cell Carcinoma. Oncol., oyad173. https://doi.org/10.1093/oncolo/oyad173.

STAR★METHODS

KEY RESOURCES TABLE

REAGENT or RESOURCE	SOURCE	IDENTIFIER
Biological samples		
Human tumors of BIONIKK trial	This study	NCT02960906
Human tumors of Pitié-Salpêtrière Hospital	This study	N/A
Deposited data		
Raw methylation and expression profiles of TCGA-KIRC cohort	NCI Genomic Data Commons[49]	https://portal.gdc.cancer.gov/projects/TCGA-KIRC
Somatic mutation and clinical data of TCGA-KIRC cohort	cBioPortal	https://www.cbioportal.org/
Copy number segmentation of TCGA-KIRC	FireBrowse	http://firebrowse.org/
Raw methylation profile of GSE61441	Wei et al.[23]	https://www.ncbi.nlm.nih.gov/geo/query/acc.cgi?acc=GSE61441
Raw methylation profile of Cancer Cell Line Encyclopedia dataset	Iorio et al.[50]	https://www.ncbi.nlm.nih.gov/geo/query/acc.cgi?acc=GSE68379
Gene expression profile of Cancer Cell Line Encyclopedia dataset	DepMap (22Q2)	https://depmap.org/portal/download/
Pre-processed methylation profile and clinical data of ccRCC-Descartes cohort	Beuselinck et al.[18]	https://www.ebi.ac.uk/biostudies/arrayexpress/studies/E-MTAB-3274
Gene expression profile of ccRCC-Descartes cohort	Beuselinck et al.[18]	https://www.ebi.ac.uk/biostudies/arrayexpress/studies/E-MTAB-3267
Gene expression profile and clinical data of CheckMate cohort	Braun et al.[11]	https://doi.org/10.1038/s41591-020-0839-y
Gene expression profile and clinical data of JAVELIN cohort	Motzer et al.[5]	https://doi.org/10.1038/s41591-020-1044-8
Software and algorithms		
R (v4.2.2)	R Core Team, 2022	https://www.r-project.org/
STAR (v2.7.10b)	Dobin et al.[51]	https://github.com/alexdobin/STAR
TCGAbiolinks (v2.26.0)	Colaprico et al.[52]	https://github.com/BioinformaticsFMRP/TCGAbiolinks
ChAMP (v2.28.0)	Tian et al.[53]	https://github.com/YuanTian1991/ChAMP
ClassDiscovery (v3.4.0)	CRAN	https://cran.r-project.org/web/packages/ClassDiscovery/index.html
KlaR (v1.7-1)	CRAN	https://cran.r-project.org/web/packages/klaR/index.html
MCPcounter (v1.2.0)	Becht et al.[54]	https://github.com/ebecht/MCPcounter
GSVA (v1.46.0)	Barbie et al.[55]	https://github.com/rcastelo/GSVA
DMRcate (v2.12.0)	Peters et al.[56]	https://bioconductor.org/packages/DMRcate/
missMethyl (v1.32.0)	Phipson et al.[57]	https://bioconductor.org/packages/missMethyl/
Limma (v3.54.0)	Ritchie et al.[58]	https://www.bioconductor.org/packages/limma/
MOVICS (v0.99.17)	Lu et al.[59]	https://github.com/xlucpu/MOVICS
clusterProfiler (v4.6.0)	Wu et al.[60]	https://bioconductor.org/packages/clusterProfiler/
RTN (v2.22.0)	Castro et al.[61]	https://www.bioconductor.org/packages/RTN/
glmnet (v4.1-4)	CRAN	https://glmnet.stanford.edu/
survival (v3.4-0)	CRAN	https://cran.r-project.org/web/packages/survival/index.html
survivalROC (v1.0.3)	CRAN	https://cran.r-project.org/web/packages/survivalROC/index.html
MEpurity	Liu et al.[62]	https://github.com/xjtu-omics/MEpurity

(*Continued on next page*)

Continued

REAGENT or RESOURCE	SOURCE	IDENTIFIER
GISTIC2.0	Mermel et al.[63]	https://www.genepattern.org
DAVID (v2023q1)	Sherman et al.[64]	https://david.ncifcrf.gov/
Enrichr	Xie et al.[65]	https://maayanlab.cloud/Enrichr/
Tumor Immune Dysfunction and Exclusion (TIDE)	Jiang et al.[27]	http://tide.dfci.harvard.edu/
Nearest Template Prediction (NTP)	Hoshida et al.[66]	https://github.com/xlucpu/MOVICS
CIBERSORTx	Newman et al.[67]	https://cibersortx.stanford.edu/
Other		
GENCODE (Release 27)	Harrow et al.[68]	https://www.gencodegenes.org/
The Molecular Signatures Database (MSigDB)	Liberzon et al.[69]	https://www.gsea-msigdb.org/gsea/msigdb
Biocarta Pathways Dataset	Nishimura et al.[70]	https://maayanlab.cloud/Harmonizome/dataset/Biocarta+Pathways
TR4	Luca et al.[71]	https://github.com/digitalcytometry/ecotyper

RESOURCE AVAILABILITY

Lead contact

Further information and request for resources should be directed to and will be fulfilled by the lead contact, Gabriel G. Malouf (maloufg@igbmc.fr).

Materials availability

This study did not generate new unique reagents.

Data and code availability

- The raw data specific to the BIONIKK trial are not publicly available due to patient privacy requirements and lack of authorization for distribution. Other data supporting the findings of this study are available from the lead contact, G.M. (maloufg@igbmc.fr), upon request. Special inquiries or requests concerning the BIONIKK trial data should also be directed to the lead contact, who will coordinate these requests in accordance with the study sponsor's guidelines.
- The public data analyzed in this study were obtained from TCGA at TCGA-KIRC, from GEO at GSE61441 and GSE68379, from ArrayExpress at E-MTAB-3267 and E-MTAB-3274, from the supplementary data files at https://doi.org/10.1038/s41591-020-0839-y for CheckMate cohort, and at https://doi.org/10.1038/s41591-020-1044-8 for JAVELIN cohort.
- The iMES R package is fully documented and freely accessible at https://github.com/xlucpu/iMES. This package offers comprehensive functions for calculating the iMES score based on the binary DNA methylation status of ccRCC patients. Additionally, it enables the classification of patients into specific regulon phenotypes. Supplementary analytic code supporting the findings of this study can be obtained from the lead contact (G.M.) upon request.

EXPERIMENTAL MODEL AND STUDY PARTICIPANT DETAILS

Sample collection and ethical approval

For the patients' samples collected from Pitié-Salpêtrière Hospital (PSL), all patients included in the PSL cohort underwent primary nephrectomy and samples with a confirmed diagnosis of ccRCC were obtained from the pathology department. The study was approved by the ethical committee of the Pitié-Salpêtrière Hospital (CPP, IDF-6, Ile de France). For the BIONIKK cohort, the study was registered with the clinical trial registry under the identification number NCT02960906. BIONIKK is a biomarker-driven trial that uses the Descartes classifications.[19] These classifications identify four tumor types (ccrcc1 to ccrcc4) based on their molecular characteristics, which are determined from transcriptomic data. These types have different responses to the drug sunitinib and show different levels of immune and angiogenic activity in the tumor environment. Specifically, tumors that respond less to sunitinib are either highly immune and inflammatory with high checkpoint expression (ccrcc4), or they have low immune activity (ccrcc1). Almost half of the tumors that respond well to sunitinib show high angiogenic and immune activity (ccrcc2). The smallest group, which also responds well to sunitinib, has features similar to normal kidney tissue (ccrcc3).[18] All patients had previously provided informed consent for tumor collection and analysis. The collection and use of tissues followed procedures in accordance with the ethical standards formulated in the Declaration of Helsinki.

METHOD DETAILS

DNA methylation and RNA-sequencing profiling

Genomic DNA and RNA were extracted from frozen samples, as previously described.[12,72] Following bisulfite conversion of genomic DNA, profiling of DNA methylation was done using the Illumina EPIC BeadArrays, as previously described.[12] Details regarding RNA-seq library preparation and sequencing were reported previously.[72]

RNA sequencing

To process the RNA-seq FASTQ files obtained from the BIONIKK clinical trial, we conducted a quality control assessment using FastQC at both the base and read levels. Samples that passed the quality control assessment were used in the subsequent analysis. The STAR aligner was then used with default parameters to generate RNA-seq BAM files with GRCh38.[51] Gene-level annotation was carried out using the GENCODE (Release 27) annotation, which was downloaded from the GENCODE project.[68] Aligned reads were summarized at the gene level using STAR. Initially, the number of fragments per kilobase of non-overlapping exon per million fragments mapped was calculated, which was then transformed into transcripts per kilobase million (TPM) values.

Public DNA methylation 450K-array cohorts

The DNA methylation profile quantified by the Illumina HumanMethylation 450K-array platform was obtained from public datasets. Specifically, 301 ccRCC samples and 160 adjacent normal tissues with available RNA-seq data were downloaded from TCGA data portal (project TCGA-KIRC), following the removal of 23 cases with molecular pathological features of MiTF/TFE translocation RCC, chromophobe RCC, and clear-cell papillary RCC.[49,73] Raw count data were downloaded using the R package TCGAbiolinks and converted to TPM.[52] Somatic mutations, clinicopathological features and OS rate data were obtained from the cBioPortal (https://www.cbioportal.org/), while copy number segment data were collected from FireBrowse (http://firebrowse.org/).

In addition, we collected raw *.IDAT files of DNA methylation 450K-array from 46 ccRCC samples with matched normal kidney tissues from the Gene Expression Omnibus (GEO) dataset GSE61441.[23] We also retrieved DNA methylation 450K-array data from the ccRCC-Descartes cohort (E-MTAB-3274), which included 102 patients with metastatic ccRCC treated with sunitinib, of which 50 patients had matched transcriptome expression profiles quantified by microarray (E-MTAB-3267).[18] The methylation profile of this cohort was pre-processed with 292,317 probes available.

DNA methylation and expression profiles for human renal cancer cell line

DNA methylation 450K-array data for human cancer cell lines were obtained from CCLE by accessing the GEO dataset GSE68379.[50] Of the 28 cell lines with the "KIRC" tumor barcode, 12 cases with available gene expression data quantified by TPM value were retrieved from the DepMap portal (https://depmap.org/portal/download/).[74]

External RNA sequencing profile from clinical trials

The transcriptome profiles for the CheckMate cohort used in this study were obtained from a previous study, which collected and combined a total of 311 tumors from patients with advanced ccRCC who were enrolled in prospective clinical trials including CheckMate-009, -010, and −025.[11] Of these patients, 181 were treated with anti-PD1 (nivolumab) and 130 with mTOR inhibition (everolimus). The corresponding OS rate data were also retrieved for these cases. In addition, transcriptome profiles and corresponding PFS data for the phase 3 JAVELIN Renal 101 trial were collected for 354 patients receiving ICI plus TKI therapy (avelumab + axitinib) from the literature.[5]

QUANTIFICATION AND STATISTICAL ANALYSIS

Quantification and filtering of DNA methylation profiles

For cohorts with available raw *.IDAT files, we used the R package ChAMP to extract the raw signal intensities and calculate the β value for each probe.[53] The β value was calculated as M/(M + U), where M and U respectively refer to the pre-processed mean methylated and unmethylated probe signal intensities. Comprehensive filtering procedures were performed using ChAMP, with the following filtering criteria applied for both 450K and EPIC arrays: removal of probes with detection of p value >0.01, probes with less than three beads in at least 5% of samples per probe, all non-CpG probes, all SNP-related probes, all multi-hit probes, and probes located in chromosomes X and Y.[75]

Definition of promoters and cancer-specific hypermethylation

The Illumina 450K and EPIC arrays share a total of 452,453 probes. Promoters were defined as regions located between −1,000 and +1,000 base pairs from the transcription start site. We investigated all CGIs loci assayed on both the Illumina 450K and EPIC platforms and determined that 96,727 (21.4%) of the promoter CGI probes for the 450K-array and 116,861 (13.5%) probes for the EPIC-array were located in promoter regions. Cancer-specific hypermethylation was further investigated for probes located in promoter CGIs that are unmethylated in normal adjacent kidney tissue, with a median DNA methylation β value of less than 0.2.

Epigenetic silencing calls

Integrative analysis proposed in our previous study was used to investigate genes that are repressed through cancer-specific DNA hypermethylation at promoter CGIs.[29] For multiple promoter CGI probes that mapped to one gene, the median β value of expression was used to represent the gene-level DNA methylation. Samples were classified as either methylated or unmethylated based on a β value cutoff of 0.3. A gene is called epigenetic silencing if, upon using the Mann-Whitney U test, it was found that the overall gene expression in methylated samples was less than or equal to that in unmethylated samples.

Identification of tumor-associated enhancer demethylator

As detailed in our recent study,[12] we selected CpG probes found in more than 50% of normal samples with a β value of at least 0.7 or probes with a median β value of at least 0.7 for both the DNA methylation 450K and EPIC arrays, in order to enrich for sites that lose enhancer methylation in cancer. For the TCGA-KIRC cohort, we reproduced the *TED* phenotype using consensus partitioning around medoids based on a total of 1,170 enhancer probes that showed high methylation levels in normal samples. For the BIONIKK cohort, we identified 12,186 enhancer probes from the EPIC platform that were highly methylated in six normal samples. Unsupervised clustering was used to identify the *TED* phenotype in ICI arms using the top 10% enhancer probes with high variability.

Copy number variation analysis

For DNA methylation EPIC-array, we used the ChAMP package to infer copy number segments from intensity values.[76] To identify recurrent focal somatic copy number alterations (CNAs), we employed GISTIC2.0 through GenePattern (https://www.genepattern.org/). Our analysis employed stringent thresholds for copy number amplifications/deletions, defined as ±0.2, with a confidence level of 0.95, and a *q* value threshold set at 0.05.[63]

Clustering analyses

For continuous data, such as the DNA methylation β matrix and transcription expression profiles, hierarchical clustering was performed using a Euclidean distance measurement with Ward's clustering method, which was implemented in the R package ClassDiscovery. For categorical data, such as regulon activity status, the *K*-modes algorithm was used to calculate the dissimilarities (total mismatches) between the data points; this was performed using the R package klaR with the default parameters.

Estimation of TME cell abundance and tumor purity

To assess the TME composition of each ccRCC case, we used the R package MCPcounter, which provides abundance scores for eight immune populations (T cells, $CD8^+$ T cells, cytotoxic lymphocytes, natural killer cells, B cell lineage, monocytic lineage, myeloid dendritic cells, and neutrophils) and two stromal populations (endothelial cells and fibroblasts).[54] To determine the functional orientation of TME, we used signatures derived from the literature,[18] including T cell activation (*CXCL9*, *CXCL10*, *CXCL16*, *IFNG*, and *IL15*), T cell survival (*CD70* and *CD27*), Tregs (*FOXP3* and *TNFRSF18*), major histocompatibility complex class I (*HLA-A*, *HLA-B*, *HLA-C*, *HLA-E*, *HLA-F*, *HLA-G*, and *B2M*), myeloid cell chemotaxis (*CCL2*), and tertiary lymphoid structures (TLSs) (*CXCL13*). We also collected four immune suppression-associated signatures,[77] including tumor-infiltrating Tregs, myeloid-derived suppressor cell (MDSC), C-ECM, and Wnt/TGF-β. Scores for each signature were calculated as the geometric mean of signature expression. The clinical response to immune checkpoint inhibitors was predicted by using TIDE, a computational framework developed to evaluate the potential of tumor immune escape from the gene expression profiles of cancer samples.[27] We applied MEpurity, a β-mixture model-based algorithm, to estimate the tumor purity based on tumor-only DNA methylation microarray data.[62]

Chromatin remodeling and vascular endothelial growth factor signatures

The *SETD2* loss signature was collected from a list of genes that are upregulated in H3K36me3-compared to H3K36me3+ (SETD2ΔN-transduced) JHRCC12 cells as well as in *SETD2*-mutant compared to *SETD2*-wildtype ccRCC from the TCGA.[40] We examined differentially accessible chromatin regions in *BAP1*-mutant tumors versus tumors without *BAP1* mutations, using data from the literature,[25] and further generated a *BAP1*-loss driven chromatin repression signature based on those genes associated with regions of reduced chromatin accessibility. The corresponding enrichment score was calculated using a single-sample GSEA (ssGSEA) approach.[55] In addition, we collected a total of 22 candidate regulators that were relevant to cancerous chromatin remodeling for regulon analysis.[78,79] Genes associated with *VEGF* were extracted from the Biocarta Pathways Dataset.[70]

Differential and enrichment analysis

Differentially methylated probes (DMPs) were identified using the standard process of ChAMP, considering a probe as significantly hypermethylated or hypomethylated if the average β value was respectively larger or smaller than other samples ($\Delta\beta > 0.2$, $p < 0.05$, FDR <0.05). Differentially methylated regions (DMRs) were identified using the R package DMRcate, considering a DMR as hypermethylated or hypomethylated if it had maxdiff >0.1 and meandiff >0.1.[56]

To perform functional enrichment analysis, we used the R package missMethyl with the MSigDB through generalized gene set testing (GGST) for both CpG and region levels of DNA methylation.[57,69] For differential expression analyses, we used the R package MOVICS with the limma approach, and for GSEA based on transcriptome expression data, we prepared a pre-ranked gene list according to the descending ordered $\log_2$FoldChange value derived from differential expression analysis, and used the R package

clusterProfiler to determine functional enrichment based on the Hallmark pathway.[59,60,80] Cytogenetic location enrichment was performed by DAVID (v2023q1).[64] Functional enrichment analysis based on the gene list was performed by Enrichr (https://maayanlab.cloud/Enrichr/).[65]

Regulon analysis

We used the R package RTN to reconstruct transcriptional regulatory networks (regulons), following the method described in a previous study.[61] Specifically, mutual information analysis and Spearman rank-order correlation deduced the possible associations between a regulator and all potential target from the transcriptome expression profile. Permutation analysis (nPermutations = 1000) was used to erase associations with an FDR >0.05. Bootstrapping strategy removed unstable associations through one thousand times of resampling with a consensus bootstrap of greater than 95%. Data processing inequality filtering eliminated the weakest associations in the triangles of two regulators and common targets. As a result, two genes, namely *ZNF280B* and *FAM19A5*, were filtered out from the initial set of 56 genes that constitute the iMES. To estimate the activity of individual regulons, a two-sided GSEA was used and the differential enrichment scores were discretized into three statuses (active = 1, wild = 0, and inactive = −1). This RTN analysis was particularly applied to the genes that correspond to the probes constituting the iMES, enabling the mirror of the iMES groups based on their collective regulon activity status. To comprehensively analyze regulon activity patterns across multiple cohorts, we employed a meta-analysis framework using a vote-counting approach, as previously described.[12] In this approach, each regulon was assigned an activity status (active, wild, or inactive), and we considered a regulon to have a specific activity status if it consistently maintained that status in regulon-suppressed phenotype versus regulon-activated phenotype in more than three out of four cohorts included in this study (TCGA-KIRC, BIONIKK, CheckMate, and JAVELIN), which had available transcriptomic expression profiles.

Development of a DNA methylation-based epigenetic silencing index

We developed an iMES using binary DNA methylation status (β value >0.2 as cutoff: 1 for methylated and 0 for unmethylated) instead of as a continuous form as it can be more easily interpretable in clinical settings and more robust to technical variation. Probes presenting with constant methylation status in a particular dataset might be attributable to platform-dependent preferential measurement, which can cause biases and may not be reproducible across datasets, or to biological bias, which failed to provide discriminative information for prognosis. Therefore, probes with constant methylation status in any datasets were removed, and probes methylated in at least 5% of the samples in a specific dataset were considered.

To minimize the risk of overfitting, we randomized the discovery TCGA-KIRC cohort into two subsets based on 5-fold sampling without replacement. The training set included 4-folds of ccRCC samples (n = 261), and the internal testing set included the rest (n = 61). We then used the glmnet R package and applied a multivariate Cox proportional hazards regression model with the ada-LASSO. This method adds weights to the traditional LASSO to counteract the known issue of bias in LASSO estimates.[81,82] 10-fold cross-validation was conducted in the training set to tune the optimal value of the penalty parameter λ that gives the minimum partial likelihood deviance—a λ of 0.599 with log(λ) of −0.513 was chosen.

Finally, a set of promoter CGI probes that were associated with silenced genes were identified, and we calculated iMES for each sample via a linear combination of the selected features, weighted by the corresponding non-zero coefficients as follows:

$$iMES_i = \sum_{j}^{n} \widehat{\beta}_j \times CpG_{ij}$$

where $\widehat{\beta}_j$ is the estimated effect size (coefficient) for probe j and CpG_{ij} is the binary DNA methylation status of the probe j in the i^{th} individual. $iMES_i$ is the i^{th} individual's computed score for iMES. Patients were dichotomized into iMES-high and iMES-low groups using the dataset-specific upper tertile as the general cutoff to achieve a comparable proportion of patients across epigenetic silencing subtypes (i.e., EPI-C1/C2 in the TCGA-KIRC and BIONIKK cohorts).

Assessment of transcriptomic signatures

For samples with available RNA-seq profiles, scores were derived for three IMmotion150 signatures, including Angio: *VEGFA*, *KDR*, *ESM1*, *PECAM1*, *ANGPTL4*, and *CD34*; Teff: *CD8A*, *EOMES*, *PRF1*, *IFNG*, and *CD274*; Myeloid: *IL-6*, *CXCL1*, *CXCL2*, *CXCL3*, *CXCL8*, and *PTGS2*.[9] The 26-gene JAVELIN Renal 101 Immuno signature includes *CD3G*, *CD3E*, *CD8B*, *THEMIS*, *TRAT1*, *GRAP2*, *CD247*, *CD2*, *CD96*, *PRF1*, *CD6*, *IL7R*, *ITK*, *GPR18*, *EOMES*, *SIT1*, *NLRC3*, *CD244*, *KLRD1*, *SH2D1A*, *CCL5*, *XCL2*, *CST7*, *GFI1*, *KCNA3*, and *PSTPIP1*.[5] The tumor inflammation signature includes *PSMB10*, *HLA-DQA1*, *HLA-DRB1*, *CMKLR1*, *HLA-E*, *NKG7*, *CD8A*, *CCL5*, *CXCL9*, *CD27*, *CXCR6*, *IDO1*, *STAT1*, *TIGIT*, *LAG3*, *CD274*, *PDCD1LG2*, and *CD276*.[30] Signature scores were calculated as the median value of Z-scored expression for the constituent transcripts. For CheckMate cohort, pre-calculated scores of Angio, Teff, Myeloid, and Immuno were collected directly from the supplementary material of the literature.[11]

Classification of Motzer's seven molecular subtypes of ccRCC

To reproduce the seven molecular subtypes previously identified in the literature, we generated a template based on genes that were specifically upregulated in each subtype (log2FoldChange >1 and adjusted $p < 0.05$). The gene signature used for this classification was derived from Genentech's profiling performed on tumors from patients enrolled in the IMmotion151 study.[6] To assign each

ccRCC case to one of the seven subtypes, we employed the nearest template prediction (NTP) approach, as previously described.[66,83] This method uses the gene expression profiles of the samples and compares them to predefined templates corresponding to each subtype, enabling accurate classification.

Cell type fraction estimation

Major cellular compartments for epithelial tumors were deconvolved using TR4, a signature matrix consisting of epithelial (EPCAM+), endothelial ($CD31^+$), fibroblast ($CD10^+$), and bulk immune cell ($CD45^+$) populations.[71] To impute cell type proportions, CIBERSORTx was applied independently to each ccRCC cohort as previously described with default parameters.[67]

Statistical analyses

All statistical analyses were conducted using R version 4.2.2. The Mann-Whitney U test was used for analyzing continuous data, while Fisher's exact test was used for analyzing categorical data. Spearman's coefficient was used for evaluating correlations between two continuous variables, and a permutation test was used to assess the significance of a correlation between a continuous and a binary variable. The permutation test involves randomly reassigning the values of the binary variable to the data points, and then calculating the correlation coefficient between the continuous and the shuffled binary variable. This process was repeated 10,000 times to create a null distribution of correlation coefficients under the assumption that there is no true association between the two variables. The observed correlation coefficient was compared to the null distribution to determine its significance, which was defined as the proportion of permuted correlation coefficients that were equal to or more extreme than the observed correlation coefficient.

Mutual exclusivity analysis was conducted using a one-sided Fisher's exact test. The statistical significance of the overlap between two groups of genes was estimated by calculating the representation factor and associated probability. The representation factor is calculated as the ratio of the number of overlapping genes to the expected number of overlapping genes based on the number of genes in each group and the total number of genes in the genome (19,620 genes annotated by GENCODE); we used the same strategy for overlapping of probes (452,453 probes shared by 450K and EPIC platforms). Representation factors of >1, <1, and 1 respectively indicate more overlap than expected from two independent groups, less overlap than expected, and that the two groups have the number of genes expected for independent groups of genes. The probability of overlapping was estimated by exact hypergeometric probability or normal approximation when the exact hypergeometric probability was difficult to calculate.

Survival rates were analyzed using Kaplan-Meier curves, with differences determined using a log rank test. Hazard ratios and 95% CI were calculated using Cox proportional hazard regression. The performance of the model was evaluated using time-dependent ROC analysis with the calculation of AUC values, using the R package survivalROC, to assess its discriminative ability in predicting the event of interest at different time points. A p-value less than 0.05 was considered statistically significant for all unadjusted analyses.